EXPERIMENTAL STUDIES ON DYNAMIC G_{IIc} OF INTERLAMINAR CRACK PROPAGATION IN CFRP

A Thesis Submitted
in Partial Fulfilment of the Requirements
for the Degree of
MASTER OF TECHNOLOGY

By
K. SURESH BABU

to the
DEPARTMENT OF MECHANICAL ENGINEERING
INDIAN INSTITUTE OF TECHNOLOGY KANPUR
JANUARY, 1991

CERTIFICATE

This is to certify that this thesis entitled "**Experimental Studies on Dynamic G_{IIc} of Interlaminar Crack Propagation in CFRP**, by **K. Suresh Babu** is a record of the work carried out under my supervision and has not been submitted elsewhere for a degree.

Prashant Kumar

(Prashant Kumar)

Professor

Department of Mechanical Engineering

Indian Institute of Technology

Kanpur-208 016

January, 1991.

NOMENCLATURE

G_c	Critical Energy Release Rate
G_{DC}	Critical Energy Release Rate Under Dynamic Conditions
$F(\Gamma)$	Instantaneous Rate of Energy Flow Through a Fixed Contour Γ Towards the Crack-Tip.
$v, \dot{a}$	Crack Velocity
B_{ij}	Coupling Stiffness Matrix
h_k	Distance from the Mid-plane to layer k.
c	Longitudinal Wave Speed
E	Young's Modulus
ρ	Density of the Material
ρc	Acoustic Impedance
$d\sigma$	Change in Stress
dV	Change in Particle Velocity
P	Applied Load
A	Area of the Load Bar
W	Work done on the Specimen
V	Particle Velocity
ε	Caliberation Strain
R_g	Gauge Resistance
S_g	Gauge Factor
R_c	Caliberation Resistance
W,b	Specimen Width

LIST OF TABLES

LIST OF CONTENTS

LIST OF FIGURES

G^{D}_{IIC} Critical Energy Release Rate in Mode II under Dynamic Conditions

C Specimen Compliance

a Crack length

K Kinetic Energy associated with the Specimen

δ Deflection of the Beam under the load P

P_c Peak Load

I Moment of Inertia of the Beam

δ_{max} Maximum Deflection of the Beam

2L Span of the Beam in 3-Point Bending

v_b Rate of Deflection of the Beam at Point x

K_l Kinetic energy in the Left Half of the Beam

V_b Maximum rate of Deflection of the Beam

CHAPTER 1

INTRODUCTION

1.1 Brief Outline :

Man has always used naturally available materials like wood, metals for various structural requirements. Alloying of metals provided an alternative to enhance the properties of metals. The requirement for improved material properties especially high strength and stiffness, large strength to weight ratio, anti-corrosive nature and performance under high temperatures opened a new class of materials - fibre composites. The attractive set of properties led to development of high strength fibers of glass, carbon and Kevlar. These found new areas of application in aeronautical, automobile and chemical industries.

Composite is an assembly of two material phases - the fibres and the matrix. The fibres provide strength while the matrix binds the fibres together. Both contribute to its lightness. Their combined nature gives performance characteristics not found in industrial constituents.

A laminated composite is prepared by stacking of plies or laminae. The fibres in the plies being in either unidirectional or woven form; with the matrix in-between to bond the layers together. The stack is subjected to a cycle of high temperature and high pressures to obtain a final laminate. Fibre orientations of neighbouring layers, in general, are not parallel to each other. The meeting plane of two such unlike plies is known as interface. Due to the anisotropic nature of the laminate, the interface forms potential site for separation of

the laminate called delamination especially under impact loads. However, various studies have shown that braiding, 3-D, 2.5-D weaving and through-the-thickness stitching offers promise for improved damage tolerance, interlaminar fracture toughness and capability to withstand out-of-plane loads .

1.2 Modes of Failure :

The modes of failure occurring in a composite depend on the properties of constituents, stacking sequence, volume fraction of fibres, loading conditions and the microstructure. A composite may fail by the following modes[1] :

(i) Breaking of fibres

(ii) Microcracking of matrix

(iii) Separation of fibres from matrix (debonding)

(iv) Delamination (separation of laminae from each other)

These modes may act jointly or separately.

1.3 Delamination :

Composites are mostly susceptible to delamination under low velocity impacts (less than the perforation velocity). This is due to:

(i) Lack of through-the-thickness reinforcement

(ii) Stress discontinuity between two plies with different fibre orientations due to the mismatch in engineering properties

(iii) Delamination or interlaminar cracks propagate in between layers due to the brittle nature of the epoxy.

The growth of delamination cracks result in progressive decrease in stiffness and residual properties of composites.

1.4 Fracture Mechanics of Delamination :

The basic principles of fracture mechanics helps in understanding the phenomenon of delamination. In fracture mechanics two approaches are adopted to study the crack growth in isotropic materials namely, the stress approach and the energy approach. Irwin[2] studied the stress field ahead of the crack-tip and formulated relations between stresses and crack lengths using a proportionality constant for the stress field, stress intensity factor K. In the second approach, Griffith[3] on the basis of energy equation,explained the criteria of fracture as the total energy change due to crack propagation in brittle materials.

The stress analysis in front of the crack tip in a composite is complex because of the local heterogeneity and anisotropy. Thus the energy approach came into practice, characterizing the interlaminar fracture by energy release rate G. G is defined as the rate of energy release per unit area of crack extension. External energy supplied causes the crack growth resulting in the formation of new surfaces. This brings in the concept of critical energy release rate G_c. G_c is that critical energy value beyond which the crack propagates. The physical parameter G is well defined mathematically and measurable in experiments. However, in evaluation of G, the material is regarded as elastic even at the crack tip. This limits its application to brittle materials in which the plastic zone at the crack tip is negligible.

J-integral approach came into prominence since it deals with the complex cases of inelasticity in metals such as plastic flow

in front of the crack tip. The J-integral is now regarded as an useful parameter in characterizing cracks in metals. Its concepts have been extended to study through-the-thickness cracks in fibre composite laminates. Like the plastic zone formation at the crack-tip in a metal, a deformed zone is formed in a laminate at the crack tip which involves matrix cracking, fibre breakage, debonding etc. On the other hand, there is only a very small damage zone in front of a interlaminar crack. Both the cracked halves generally remain elastic leaving only a thin matrix zone between the two plies to deform excessively. The crack extension at the tip is complex possibly with multiple cracks and its mechanisms are not understood so far. Since most of the deformation in a laminate is elastic it has been a common practice to use G as the characterizing parameter for interlaminar crack growth.

1.5 Modes of Interlaminar Failure :

In general, the interlaminar failure may occur by any one of the three modes- mode I, mode II or mode III (figure 1.1). Mode I failure (opening mode) occurs when stress is applied at right angles to the laminate plane in opposite directions resulting in opening of the laminate. Mode II failure (forward shear mode) is caused by in-plane shear stresses as in the case of 3-point bending. Mode III is a rare failure mode (parallel shear mode) due to the anti-plane shear stresses.

Experiments have shown that a mixed mode failure occurs due to the combination of normal and interlaminar shear stresses depending on the laminate configuration and the loading conditions. An approach which could characterize the resistance

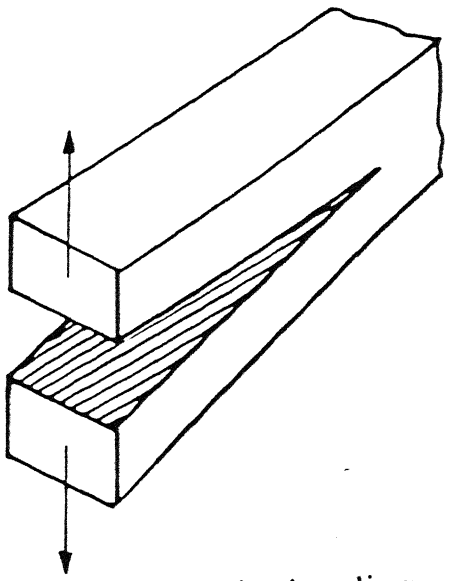

(a) Mode I: symmetric loading
(opening mode)

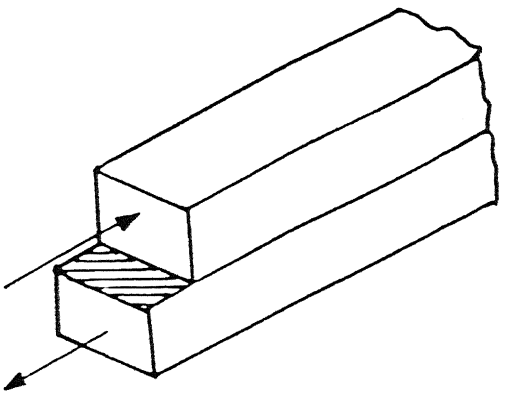

(b) Mode II : skew symmetric
shear loading
(forward shear mode)

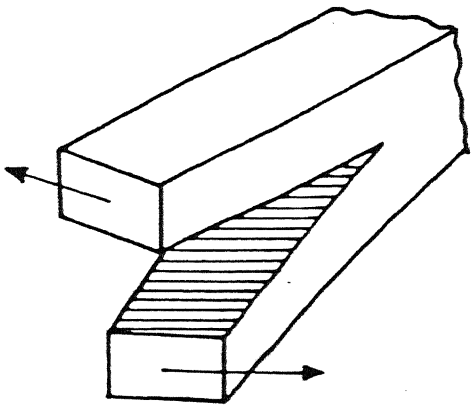

(c) Mode III : antiplane shear loading
(parallel shear mode)

Fig. 1.1 Modes of Crack Surface Displacement

of a material to opening and shear modes is of prime importance.

1.6 Impact :

The absence of through-the-thickness reinforcement makes a laminated composite most vulnerable to impact damage. The toughness values in composites are quite low which determine the amount of energy absorbed during impact. Low velocity impacts which do not penetrate the material cause damage over a large area mostly through delamination. Structures made from composite materials such as body frames, I-sections having fixed or free boundaries are mostly subjected to lateral loads under service conditions.

The cracks initiate and propagate delamination through several mechanisms such as:

(i) Transverse cracks are nucleated on free surfaces by flexural loads which move inside and within the surface ply. They gain energy as they move. When they reach an interface they turn sideways, i.e. they become interlaminar cracks.

(ii) Foilage occurs at the rear most interface caused by the tensile pulse generated at the rear free surface.

(iii) High shear stresses nucleate and propagate cracks near the mid plane.

The first two mechanisms cause crack propagation mostly in mode II while the foilage in the third mechanism is mainly developed in mode I. Thus the study of dynamic mode I and mode II delamination for different composite materials is necessary to understand the material response and take definite approaches to improve interlaminar fracture toughness or delamination resistance. In this study only dynamic crack propagation in mode

II is considered.

1.7 Dynamic Energy Release Rate :

The dynamic release rate is defined as the rate of mechanical energy flow out of the body and into the crack tip per unit crack advance per unit thickness of the body in the direction perpendicular to the plane of deformation. Consider a crack extending with a velocity v as shown in figure 1.2 . Around the region of the crack-tip, τ is a small contour surrounding the tip and connecting the two traction free surfaces[4] .It is fixed both in size and orientation in the crack-tip reference frame as the crack grows.

In analytical terms, the critical energy release rate under dynamic conditions is

$$G_{DC} = \lim_{\tau \to 0} \left\{ \frac{F(\tau)}{v} \right\} \qquad (1.1)$$

where $F(\tau)$ is the instantaneous rate of energy flow through the fixed contour τ towards the crack tip and v is the crack velocity. The limit applies that the contour τ shrinks onto the crack tip. The values calculated according to equation 1.1 are independent of the shape of τ.

The formulation is based on energy balance and the mechanical energy is the sum of elastic strain energy and kinetic energy stored in an elastic body. The kinetic energies of rotary inertia and shear deformation are much smaller than the strain energy and are neglected.

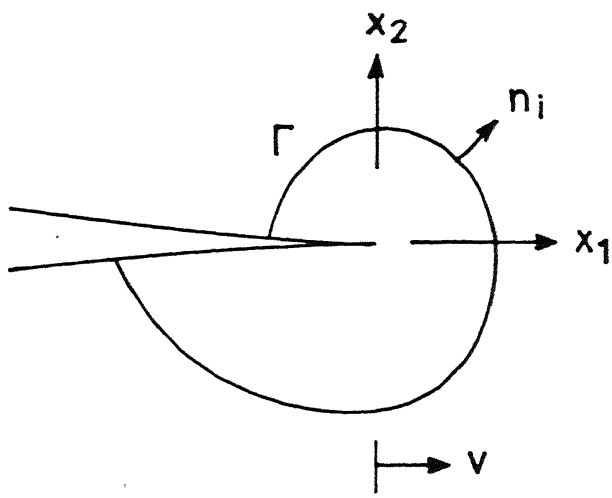

Fig. 1.2 The contour Γ around the crack-tip moves with velocity v .

CHAPTER 2

LITERATURE SURVEY

A number of methods have been proposed to characterize the resistance to delamination in composites under shear loading based on bending tests using a starter crack to promote shear failure. The testing methods include[5] :

(i) End Notch Flexure (ENF) test

(ii) End Loaded Split (ELS) test for thin specimens

(iii) End Notched Cantilever Beam (ENCB) test for thick specimens

(iv) Cantilever Beam Enclosed Notch (CBEN) test.

Figure 2.1 shows the schematic diagrams of Mode II bending tests.

The ENF test has received considerable attention for examining the flexural properties. The bending fixture is simple and the test may be performed on thin specimens. However, a minimum thickness is required to avoid flexural failure and ensure the applicability of small displacement beam theory. The crack length and the span of the specimen is always adjustable, making it the most flexible of all the Mode II tests.

Depending on the nature of the experimentation, different sets of dimensions were selected by various researchers.Carlsson et.al.[6] used end notched flexure (ENF) specimens to find Mode II energy release rates for different thickness to span ratios, neglecting inter-laminar shear deformation. The expression for G_{IIC} was derived using short deflection beam theory and a

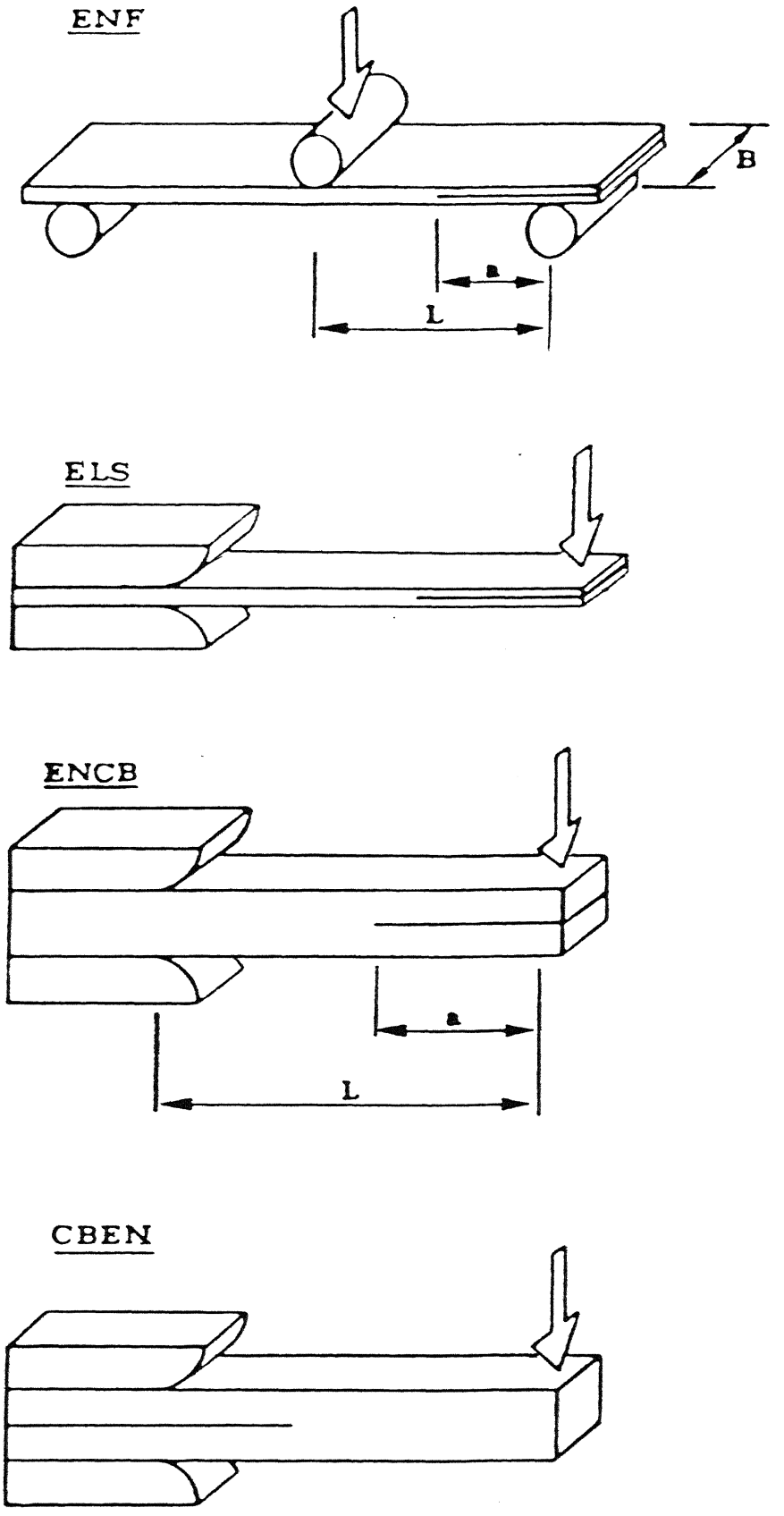

Fig.2.1 Schematic diagrams of Mode II bending tests: (a) End Notched Flexure, (b) End Loaded Split (thin) or End Notched Cantilever Beam (thick): (c) Cantilever Beam Enclosed Notch.

numerical analysis was conducted. The influence of geometrical and material properties on G_{IIC}, the criteria for the crack to be unstable and the crack propagation due to friction between the crack surfaces is vividly described. Moron and co-workers[7] also used ENF specimens to determine mode II interlaminar fracture toughness for various types of fibre reinforcement. Maikuma et.al.[8] studied the mode II delamination, using centre notched flexure (CNF) specimens, in four types of carbon fibre reinforced polymer matrix composites. The G_{IIC} values were determined experimentally, analytically and also using finite element analysis. On comparison between ENF and CNF test methods analytically, excellent agreement was obtained. Davies et.al.[9] examined the delamination resistance of unidirectional carbon/epoxy composite. The results of a round robin exercise involving 10 laboratories are presented. They found that the mode II initiation values depended on the starter film thickness, lower values with less scatter for thin films while the propagation values were reproducibly measured. The Mode II value was also found to depend on specimen width.

Little work has been carried out in the area of dynamic Mode II fracture in composites. Smiley and Pipes[10] investigated the rate sensitivity of composite specimens in Mode II for a range of cross head speeds. Under impact at slow speeds the behaviour was ductile with plastic deformation and at high speeds brittle fracture with little crack growth. The G_{IIC} values decreased on increase of shear displacement rate due to decrease in development of plastic deformation during loading.

The delamination fracture toughness of graphite/epoxy

impact loading was studied by Sun et.al.[10]. For a short beam specimen, the relation between impact force and strain response is complicated by the fact that flexural waves are dispersive. An indirect method using finite element analysis, the contact force history was obtained. The maximum value of G provided by impact at the threshold velocity (minimum velocity at which the crack extends) is taken as critical G. The Mode II was found to be predominant and the valuesof G obtained were much higher than for the quasi-static case.

Maikuma et.al.[11] repeated the investigation of Mode II interlaminar fracture of composites under impact loading. Their model was based upon the beam theory including kinetic energy contribution and dynamic finite element analysis along with virtual crack closure techniques. In experimentation, CNF specimens were tested in 3-point bending in the instrumented drop weight tester. The initiation and propagation toughness values were found to be smaller than the corresponding quasi-static values.

In this study carbon/epoxy specimens with an edge artificial crack were prepared in the laboratory from sixteen layers of unidirectional fabric. The specimen was subjected to 3-point bending by a load bar, in which a square shaped stress pulse was generated. The rate of energy input to the specimen was determined by recording the incident and reflected pulses in the load bar. The crack velocity was measured by the propagation gauges bonded in front of the crack tip. By knowing the rate of energy input to the specimen and the crack velocity the energy release rate was evaluated.

In chapter 3, specimen preparation described in detail, is applicable particularly for this technique. Chapter 4 concerns with the working of the technique in Mode II testing. The results and discussions are dealt in chapter 5. Finally the conclusions are given in chapter 6.

CHAPTER - 3

SPECIMEN PREPARATION

Carbon/epoxy specimens having ENF configuration were prepared in the laboratory by the hand lay-up technique. Mode-II precracking of the specimens was done in fatigue. Propagation gauges were bonded on the specimen in front of the crack tip to measure the crack velocity.

3.1 Hand Lay-up Technique

Unidirectional carbon fabric(G-808) with warp to weft ratio of 91:9 was cut to obtain 16 layers of size 160 X 160 mm and the desired angle. Epoxy (LY556), hardener (HT1907 IN) and accelerator (DY062) were weighed in the ratio of 100:85:1.5. Using a brush (width 25 mm) a thin layer of this mixture was applied over each layer by keeping one layer above the other in a desired sequence. A thin BOPP(Bi-axially oriented polypropylene, thickness 20 μm and width 30mm) was kept between the eighth and ninth plies to obtain an artificial crack at the centre. The orientation code of the laminate is shown in figure 3.1.

3.2 Orientation Code of the Laminate

The salient features of the stacking sequence are :

(i) The coupling stiffness matrix [B] is null.

(ii) Presence of an interface at the centre of the laminate.

(iii) The overall laminate is unsymmetric. However the halves about the mid plane are symmetric.

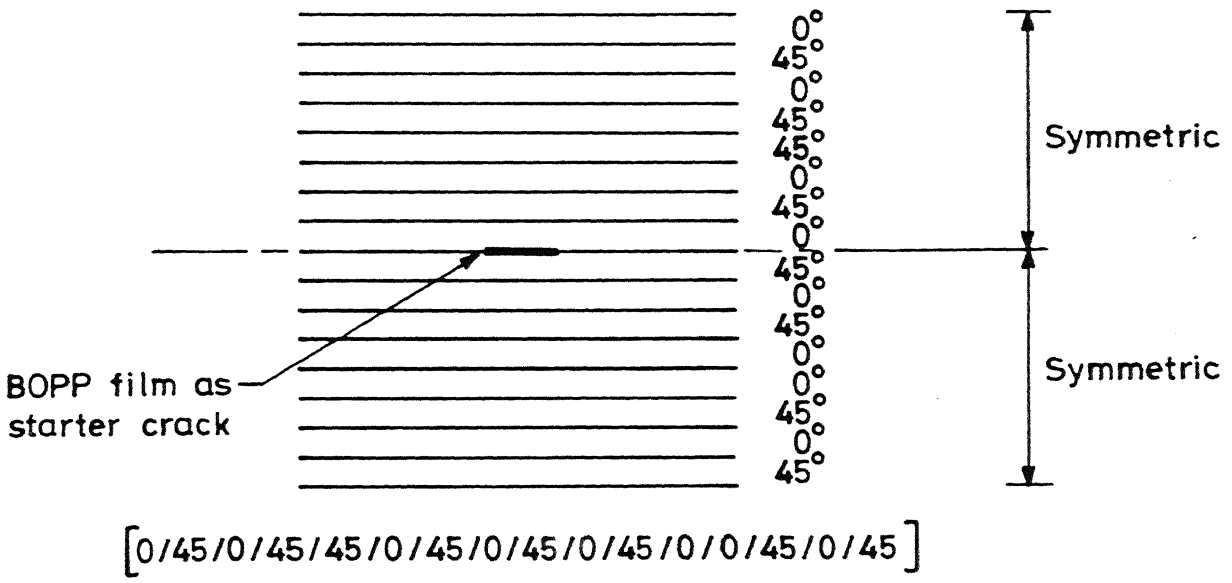

Fig. 3.1 Orientation code of the laminate.

(iii) The overall laminate is unsymmetric. However the halves about the mid plane are symmetric.

The coupling stiffness matrix for the given orientation is given by :

$$B_{ij} = \frac{1}{2}\sum_{K=1}^{16} (\bar{Q}_{ij})_k (h_k^2 - h_{k-1}^2)$$

$$= \frac{1}{2}\Big[(\bar{Q}_{ij})_0((-7)^2 - (-8)^2) + (\bar{Q}_{ij})_{45}((-6)^2 - (-7)^2)$$
$$+ (\bar{Q}_{ij})_0((-5)^2 - (-6)^2) + (\bar{Q}_{ij})_{45}((-4)^2 - (-5)^2)$$
$$+ (\bar{Q}_{ij})_{45}((-3)^2 - (-4)^2) + (\bar{Q}_{ij})_0((-2)^2 - (-3)^2)$$
$$+ (\bar{Q}_{ij})_{45}((-1)^2 - (-2)^2) + (\bar{Q}_{ij})_0((-0)^2 - (-1)^2)$$
$$+ (\bar{Q}_{ij})_{45}(1^2 - 0) + (\bar{Q}_{ij})_0(2^2 - 1^2)$$
$$+ (\bar{Q}_{ij})_{45}(3^2 - 2^2) + (\bar{Q}_{ij})_0(4^2 - 3^2)$$
$$+ (\bar{Q}_{ij})_0(5^2 - 4^2) + (\bar{Q}_{ij})_{45}(6^2 - 5^2)$$
$$+ (\bar{Q}_{ij})_0(7^2 - 6^2) + (\bar{Q}_{ij})_{45}(8^2 - 7^2)\Big]$$

$$= \frac{1}{2}\Big[(Q_{ij})_0\{49 - 64 + 25 - 36 + 4 - 9 - 1 + 3 + 7 + 9 + 13\}$$
$$+ (Q_{ij})_{45}\{36 - 49 + 16 - 25 + 9 - 16 + 1 - 4 + 1 + 9 - 4$$
$$+ 36 - 25 + 64 - 49\}\Big]$$

On simplification

$$B_{ij} = 0$$

For the laminate, the bending-stretching coupling is eliminated. On application of bending moment to this laminate produces only bending strains but no mid plane strains. The mid plane of the laminate forms the plane of delamination. Hence an artificial delamination crack is made here.

3.3 Preparation of the Laminate :

The stacking obtained by the hand lay-up technique was covered by the BOPP films, one above and another below it and four pieces of woolen felt (thickness-6 mm) along the edges of the stack so that the excess epoxy was readily absorbed . The assembly is placed between two aluminium plates (240 X 240 X 15 mm) and kept in between the two plates of the hot press.

A pressure of 0.29 MPa was applied using a pump attached to a hydraulic jack of 20 ton capacity[13]. The heating elements which are thermostatically controlled, are switched on to their 100% efficiency. The temperature of the laminate was measured using a copper-constantan thermocouple. The end of the thermocouple was embedded near the edge of the stacking before being compressed. The generated DC voltage due to the increase in temperature was measured using a digital multi-meter. The schematic view of the press is shown in figure 3.2.

The multi-meter reading was allowed to increase to a value of 5.4 mV corresponding to a temperature of 150^{o}C of the stacking. At this temperature, the epoxy mixture becomes highly viscous toform a gel. The pressure was then raised to 0.98MPa .The efficiency of the thermostat element was brought down to 42%. This rate of heating and cooling enabled a constant temperature of 150^{o}C to be maintained. After an hour, the thermostat was switched off and the laminate assembly was allowed to cool down to room temperature in the hot press at the same pressure.

The laminate was taken out and the release films and felt pieces were removed. The plate was cut to obtain CNF (centered

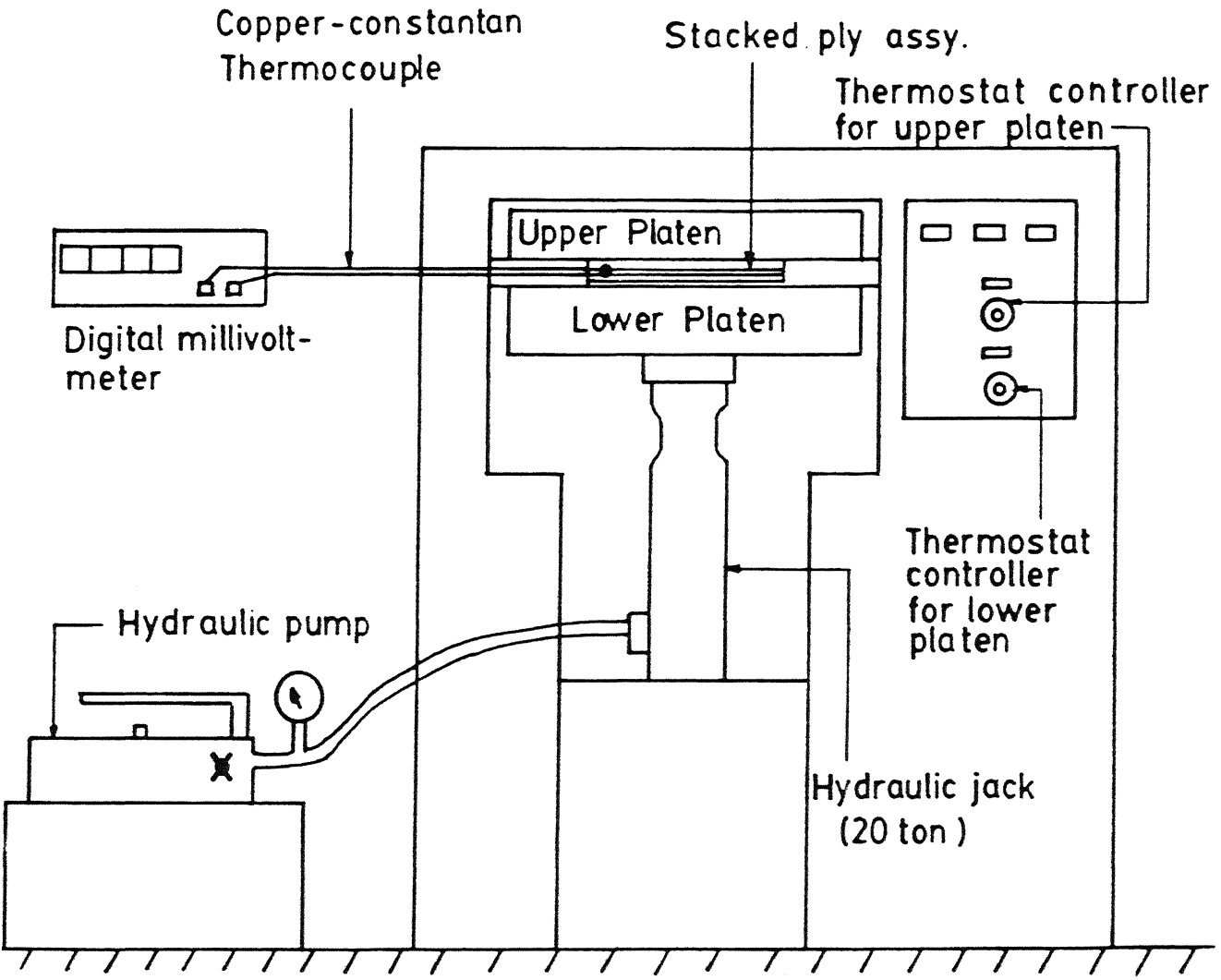

Fig. 3.2 Schematic View of the Press

notched flexure) specimens using a diamond cutter, cooled by running water. The specimens were then polished on their sides using emery papers of 150 grits.

3.4 Preparation of Specimen :

In order to obtain a sharp crack tip, precracking of specimens is important before conducting the flexural test. As a blunt crack-tip absorbs more energy, precracking ensures uniformity among the crack tips of all specimens.

The sharpening of crack is done in mode-II by subjecting the CNF specimens to fatigue loading. The specimen was loaded on the Material Testing System (MTS 80, Capacity-10 ton) in 3-point bending having a span of 40 mm (the load was slowly increased under 10% stroke controlled condition until the crack extended. A plot between the load and displacement for above specimen gives the ultimate strength in flexure.

The maximum load for fatigue testing was selected to be 60% of the ultimate load. The minimum load was 10% of the maximum load. A frequency of 5 Hz gave sufficient time for the crack to propagate. Fatigue test was done under load control.

Each specimen was coated with whitener in front of the starter crack for about 10 mm. The specimen was subjected to fatigue loading as shown in figure-3.3. Either side of the centre crack was extended individually so that one could control the distance travelled by each crack-tip. A magnifying lens and a table lamp helped to accurately monitor the propagation of the crack-tip. The crack grew against a white background and when

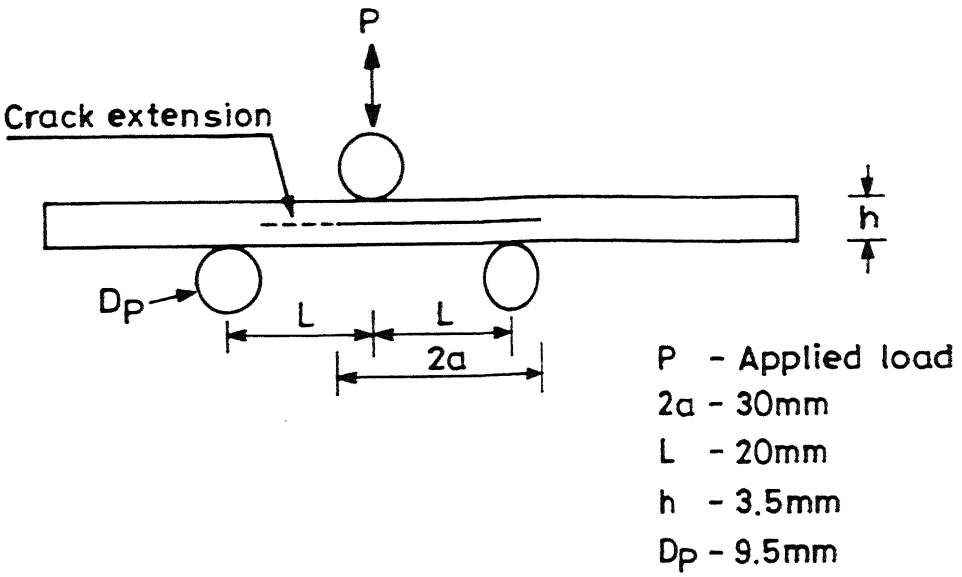

Fig. 3.3 Precracking CNF specimen under 3-point bending in fatigue, one crack-tip at a time.

the crack attained a length of approximately 10 mm, the load was slowly released.

From each CNF specimen, two ENF specimens were obtained whose dimensions are shown in figure-3.4.

3.5 Propagation gauges :

Propagation gauges were developed in the laboratory using thin wires of copper carrying electric current. Four grooves of depth 0.2 mm were made in a specimen starting from the crack-tip at a distance of 0.5 mm. Thin copper wires (diameter 28 μm) after degreasing, are placed one each in a groove and then bonded to the specimen by epoxy mixture (i.e. epoxy (LY556) and hardner (HY951) in the ratio of 100:14). The tension in the wire was maintained using press blocks and small C-clamps.

After curing, a thin crack-tip was made in the epoxy layer using a sharp razor blade along the starter crack as shown in figure 3.5 . Also, a groove was cut in the epoxy bond layer as shown, to facilitate crack propagation. After checking the continuity of propagation gauges using a multi meter, the ends of the propagation wires were soldered to a relatively thicker copper wire (diameter 60 μm) to be connected to an oscilloscope through a logic box to be explained in chapter 4.

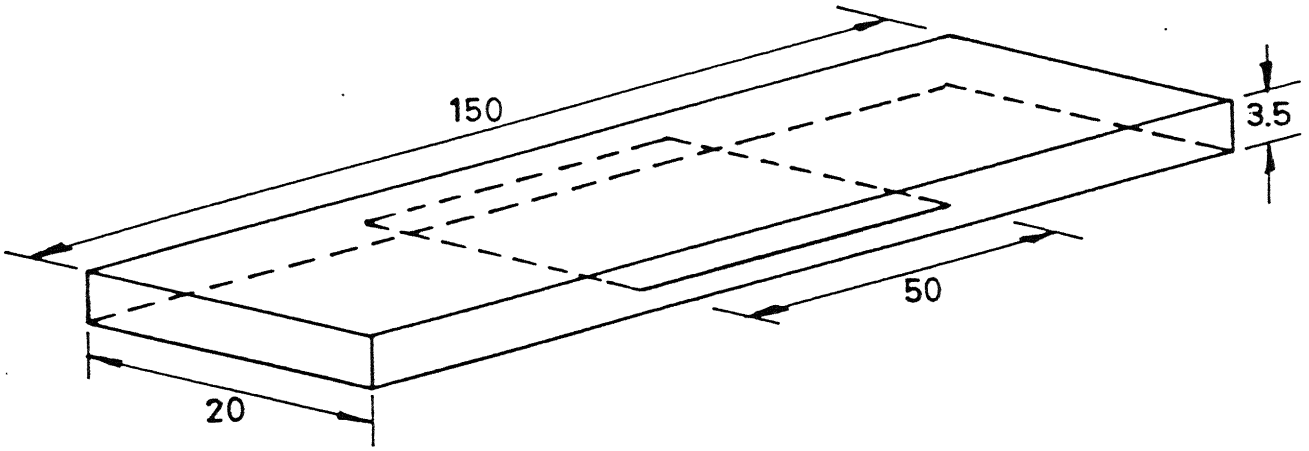

(a)

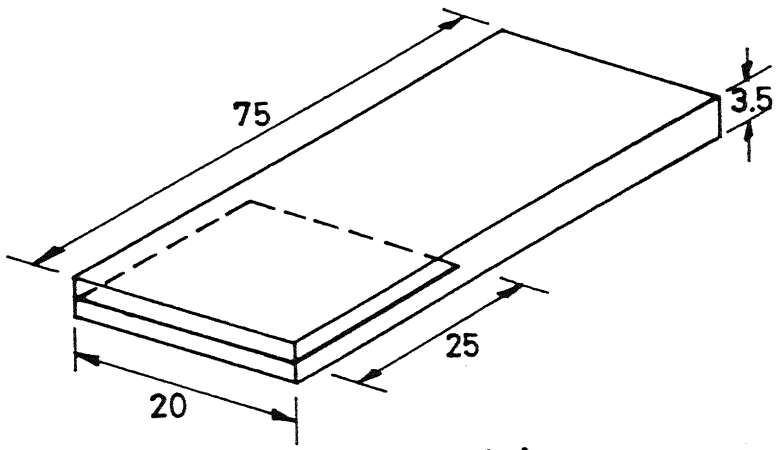

(b)

Fig. 3.4 (a) Geometry of CNF after precracking,
(b) Geometry of ENF specimen .

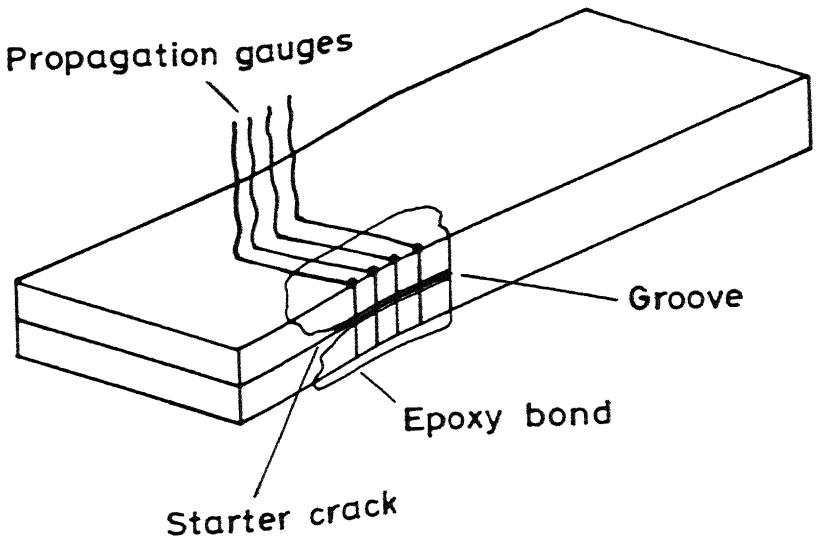

Fig. 3.5 Specimen with propagation gauges.

CHAPTER - 4

DYNAMIC MODE-II TESTING

4.1 Introduction

ENF specimens were tested in a three point bend testing fixture with a load bar under dynamic conditions. The schematic view of the experimental setup is shown in figure 4.1 . The striker accelerated in the air gun, gains a velocity around 6 m/s and impacts the load bar. A compressive stress pulse is generated at the point of impact in the load bar which traverses the length of the bar. At the end of the bar, part of the energy is given to the specimen and the remaining is reflected as a reflected pulse. The work done on the specimen goes to increase the strain energy of the specimen, formation of new cracked surfaces and provides kinetic energy to the specimen. The specimen is supported over two rigid supports which absorb negligible energy. The record of incident and reflected pulses by strain gauges bonded to the load bar provides the energy input to the specimen. The crack velocity is measured through the propagation gauges infront of the crack tip. The experimental-setup of dynamic mode II testing is shown in figure 4.2 .

4.2 Elastic Wave Propagation in the Load Bar :

The determination of energy input to the specimen is based on the theory of one dimensional elastic wave propagation in circular load bars. On impact, the load bar remain elastic as the

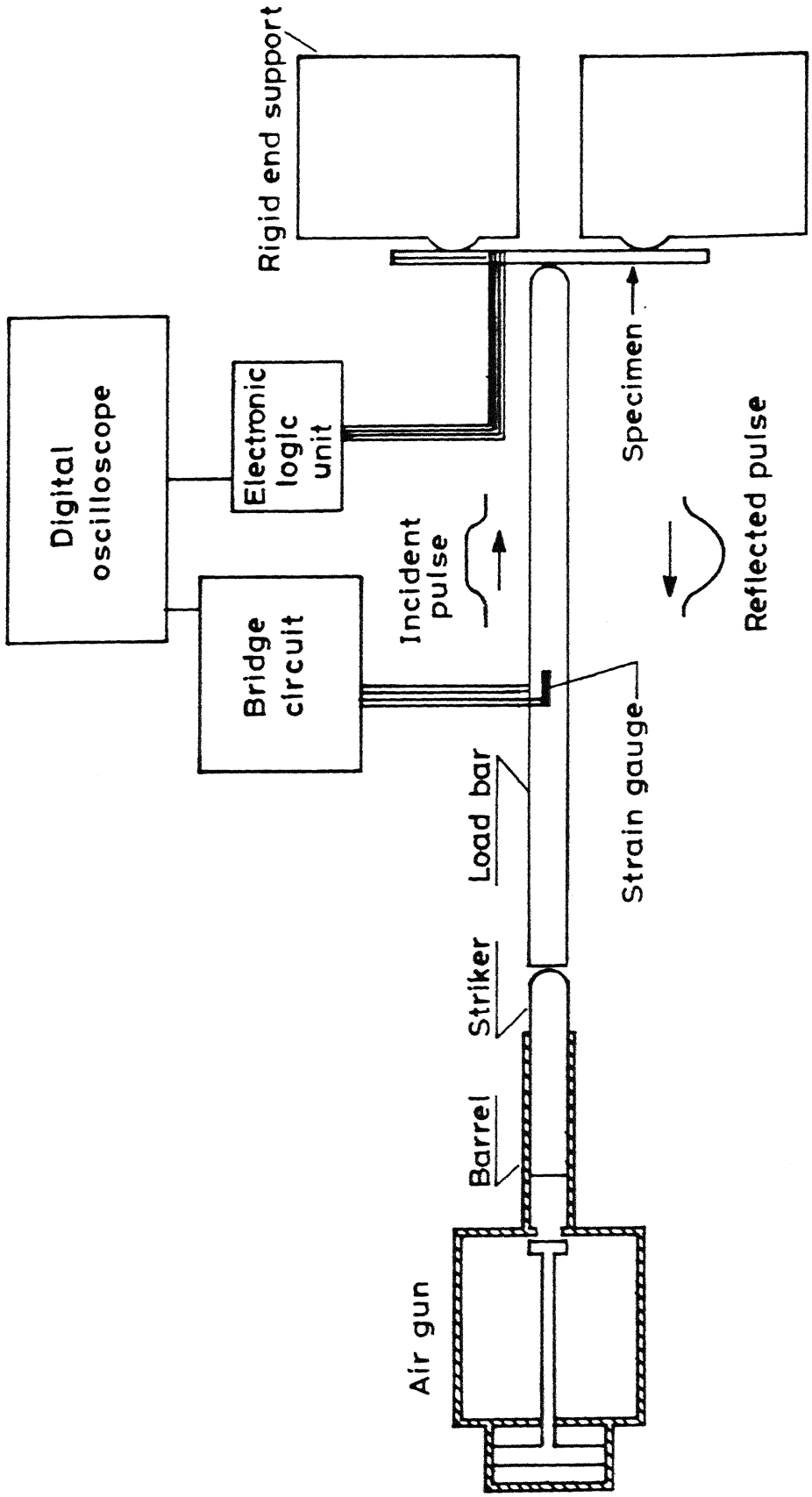

Fig.4.1 Schematic diagram of the experimental setup.

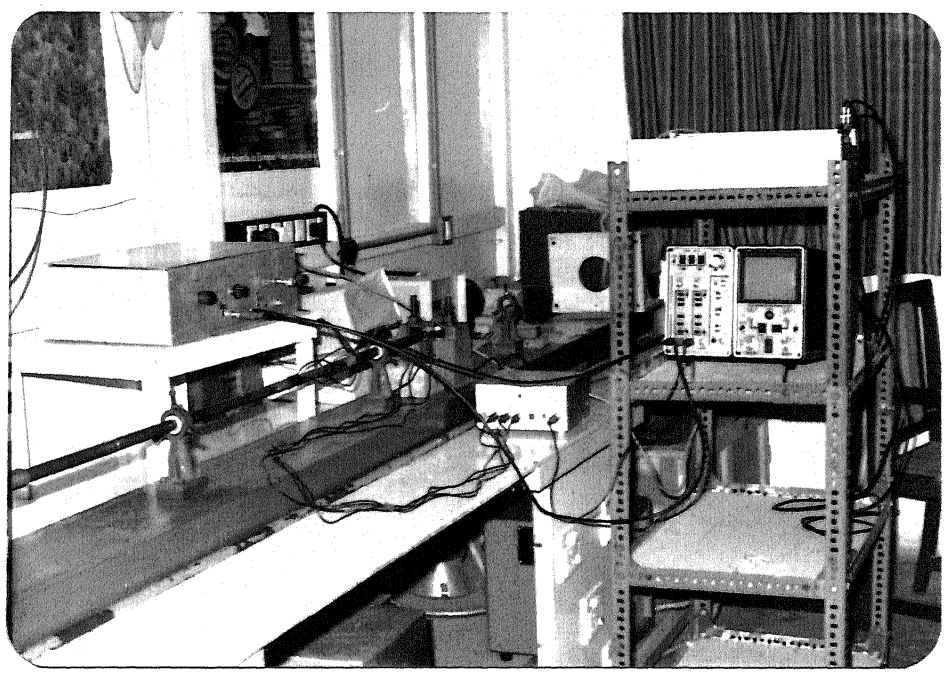

Fig. 4.2 The Experimental Setup for Mode-II Testing

stresses are low. Further the wave propagation is nondipersive in the chosen circular cross-section of the bar. This facilitates application of one dimensional elastic stress waves to determine the load and particle velocity at the midpoint of the specimen by the load bar[14].

The incident and the reflected pulses are sensed by the strain gauges mounted on the load bar and recorded by the digital oscilloscope. The gauges are placed at a sufficient distance so that by the time the reflected pulse arrives at the strain gauges, the incident pulse dies down and the two pulses are cleanly recorded without an overlap or interference. The distance is decided by the longitudinal wave speed (c) given by $(E/\rho)^{1/2}$ where E and ρ are Young's modulus and density respectively. For carbon steel, the wave speed is 5.15 mm/μs.

The next section discusses how the load on the specimen and the particle velocity at the midpoint of the specimen are determined from the record of the incident and reflected pulses.

4.3 Evaluation of Stress and Particle Velocity :

Stress wave propagation in the load bar is shown through a time - distance diagram as in figure 4.3. Applying one dimensional stress wave theory for a linear elastic material, the wave equation along characteristic direction are[15] :

$$d\sigma - \rho c dV = 0 \qquad \text{along positive characteristic}$$

$$d\sigma + \rho c dV = 0 \qquad \text{along negative characteristic}$$

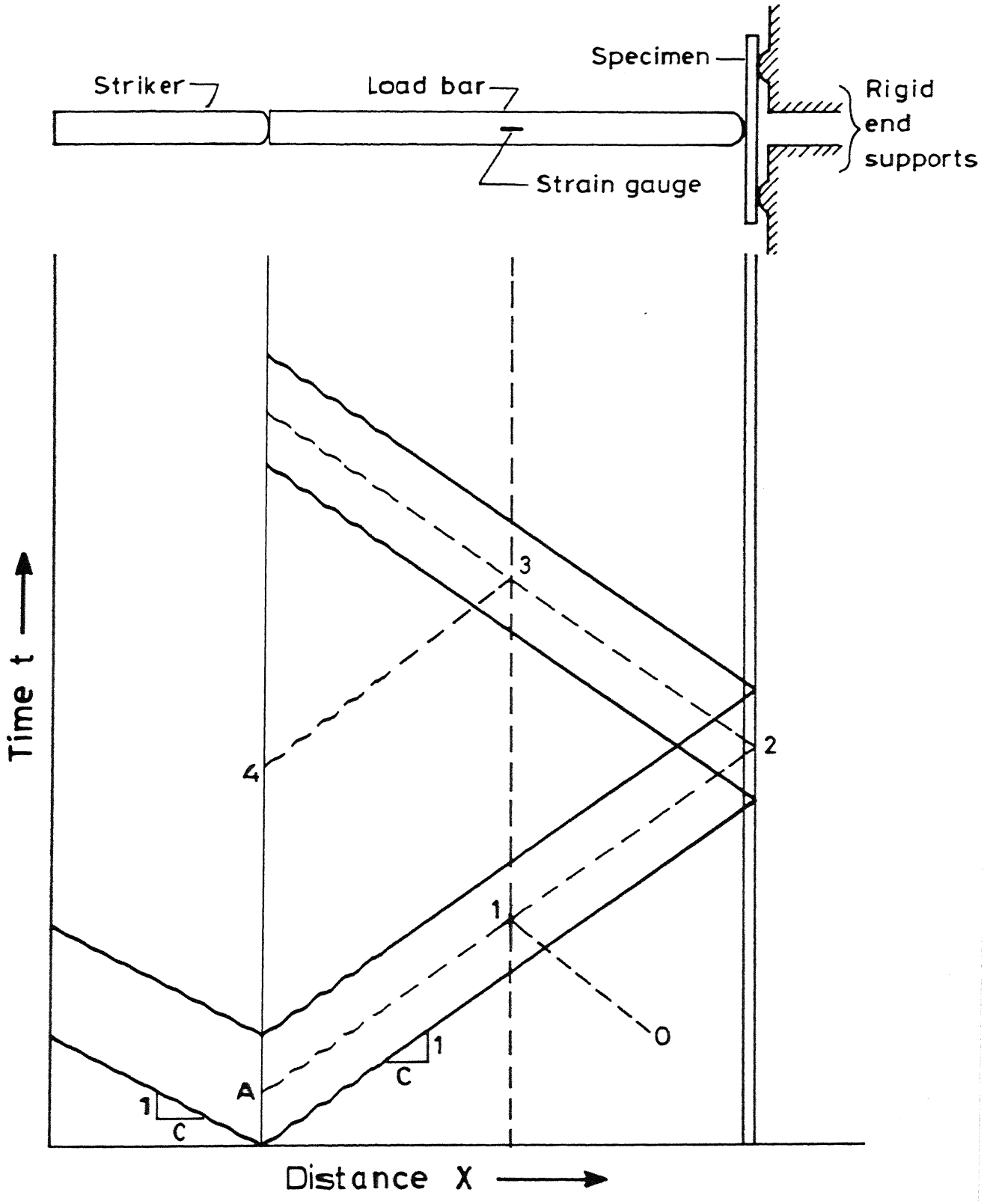

Fig. 4.2 Time - distance diagram.

where $d\sigma$ and dV represent the change in stress and particle velocity respectively and the product ρc is called the acoustic impedance of the material.

Along path 1 – 2, one obtains

$$\sigma_1 - \rho c V_1 = \sigma_2 - \rho c V_2 \qquad (4.1)$$

For the path 2 – 3, the relation becomes

$$\sigma_2 + \rho c V_2 = \sigma_3 + \rho c V_3 \qquad (4.2)$$

Since the load bar was at rest with no internal stresses just before the impact , the relation along the characteristic 1 – Ø provides

$$\sigma_1 + \rho c V_1 = Ø \qquad (4.3)$$

The striker and the load bar are made of the same material and of the same diameter. In such symmetrical impacts, once the compressive pulse generated at point A makes a round tip to the rear end of the striker and comes to the interface, the stress and particle velocity becomes zero at the interface. The relation along 3 – 4 simplifies to

$$\sigma_3 - \rho c V_3 = Ø \qquad (4.4)$$

Substituting the values of V_1 and V_3 from equation (4.3) and (4.4) in equation (4.1) and (4.2) respectively, one obtains

$$\sigma_2 - \rho c V_2 = 2\sigma_1 \qquad (4.5)$$

$$\sigma_2 + \rho c V_2 = 2\sigma_3 \qquad (4.6)$$

From the above two equations, the stress and particle velocity at point 2 are :

$$\sigma_2 = \sigma_1 + \sigma_3 \qquad (4.7)$$

$$V_2 = \frac{\sigma_3 - \sigma_1}{\rho c} \qquad (4.8)$$

The point 2 corresponds to the specimen face with the incident bar. The load applied on the specimen becomes

$$P_2 = (\sigma_1 + \sigma_3) A \qquad (4.9)$$

Where A is the area of load bar.

At any time t, the stress (σ_2) and particle velocity (V_2) are known from the instantaneous values of σ_1 and σ_3. For a time duration of (0-t)μs, the work done on the specimen is given by

$$W = \int_0^t P_2 V_2 \, dt \qquad (4.10)$$

4.4 The Supports :

The specimen is supported by two heavy steel blocks which are held rigidly to the base channel of mild steel. Two carbon steel pins of 10 mm diameter and 24 mm long are brass soldered at the top of both the blocks, one on each block. These two pins work as end supports of the specimen. The two blocks are positioned in such a way that the span between the two pins is 50 mm and the pin on the load bar is equidistant from either pin. The supports are so rigid that they absorb negligible energy.

4.5 Air Gun :

The air gun provides a mechanism of accelerating the striker. The advantage of using the air gun lies in the fact that a desired velocity of the striker can be obtained.

The air gun available in the laboratory has been specially designed to conduct dynamic experiments (figure 4.4).The breech assembly which stores high pressure nitrogen gas is equipped with a quick opening mechanism as well as a control panel to fire the gun. The gun barrel has a diameter of 19.8mm and a length of 1680mm. The internal surface of the barrel is polished using different grades of sand paper from coarse to fine and a light lubricant is applied .The desired velocity is obtained by controlling the pressure given to the air gun through a control panel.The striker has a diameter of 19mm and a length of 281mm. It is made of carbon steel weighing 0.653 kg. The striker is inserted in the barrel using a stiff copper wire. In order to prevent leaking of the compressed nitrogen gas through the sides

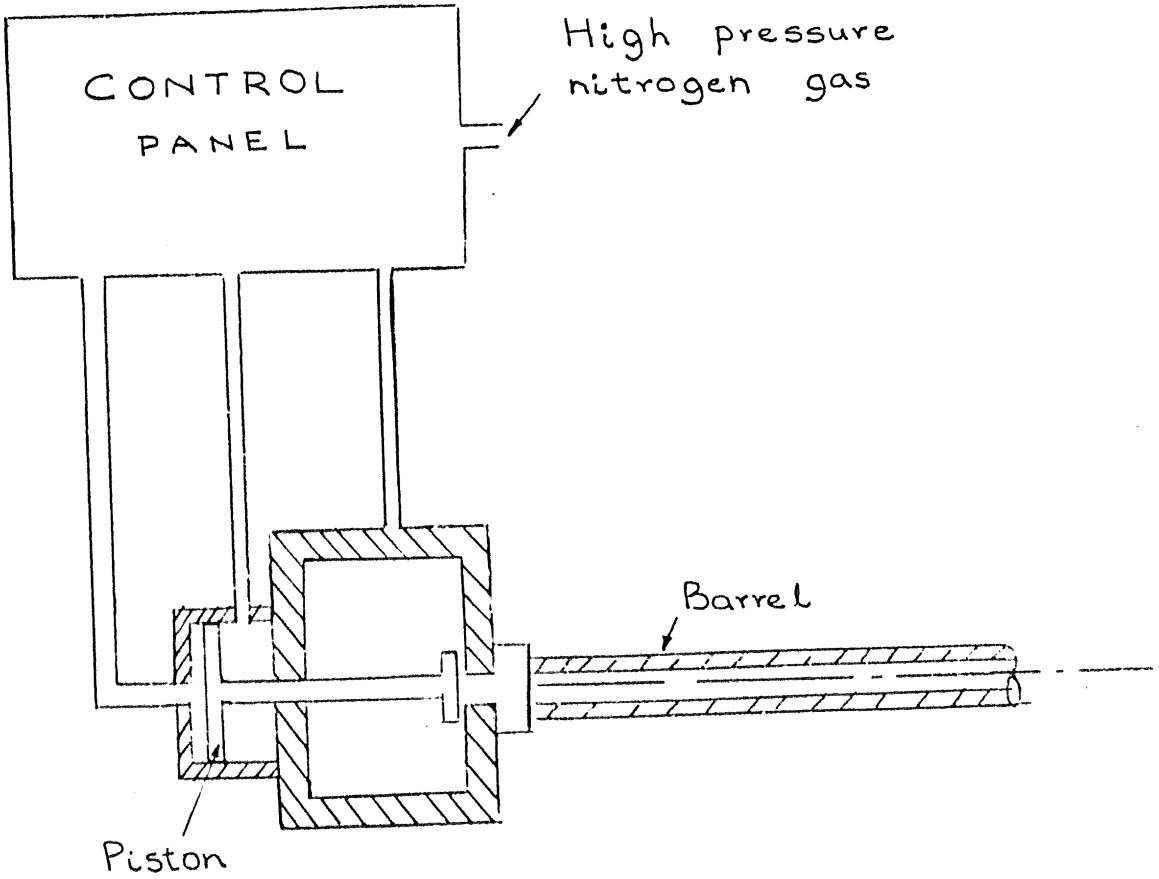

Fig. 4.4 View of the Air-Gun

of striker, an 'O'ring is provided on a suitably designed groove close to the rear end. The 'O' ring is kept lubricated with the silicone vacuum grease.

The velocity of the striker coming out of the barrel is measured through an optical system. Three light beams are emitted, from IEE 387 bulbs installed at an interval of 15mm in a aluminium block attached at the front end of the barrel. Each light beam is recieved by a photo-diode (SI 100) embedded on the other side of the aluminium block such that the the striker passes between the bulb and the photo-diode. The photo-diodes are connected to the time counter capable of measuring time with an accuracy of 1μs. As the projectile cuts the first light beam the first screen of the counter starts counting; when the striker cuts the second beam,first screen of the counter stops counting and the second screen starts.Similarly the third screen starts and the second stops when the striker cuts the third beam.The third screen just notes the instant of time . Thus by knowing the distance between the light beams and the time time taken by the striker, the velocity of the striker is determined.

4.6 Recording of Stress Pulses :

The impact of the striker with the load bar produces stress pulses in the load bar.As a result the bar undergoes longitudinal deformation.The strain gauges bonded on the load bar are also deformed simultaneously. The longitudnal strain of the load bar is proportional to the change of resistance of the strain gauges. This resistance change is seen as potential change in the oscilloscope when connected through a balanced Wheatstone

bridge. The circuit of the Wheatstone bridge is shown in figure 4.5. The strain gauges sense the stress pulses and the resulting resistance change in the already balanced circuit varies in accordance with the nature of the pulse. The digital oscilloscope digitizes the potential changes in the circuit and records the incident and reflected pulses.

The digital oscilloscope (Nicolate 2090 III) has two independent channels . Each of these channels were used to record the stress pulses and the crack growth rate seperately.Triggering of the oscilloscope was done internally through the snapping of the first propagation gauge.As anin-built feature of the oscilloscope the last stress pulse is recorded just before the oscilloscope is triggered. The oscilloscope has a sensitivity of 0.5μs on its time scale.

4.7 Measurement of Crack Velocity :

The crack velocity or the rate of the crack growth is determined by the propagation gauges bonded infront of the crack tip[16]. The specimen deflects in three point bending under an impact load of the load bar. This causes the sliding of the two halves of the laminate about the midplane resulting in propagation of the crack.The extending crack breaks the propagation gauges,one by one in a sequence.This causes potential drops in the electronic logic unit circuit to be recorded by the oscilloscope.

The circuit of the electronic logic unit is shown in figure 4.6 . It consists of integrated chips, resistances and condensors to give a sharp response time (less than 0.5 μs). The reset

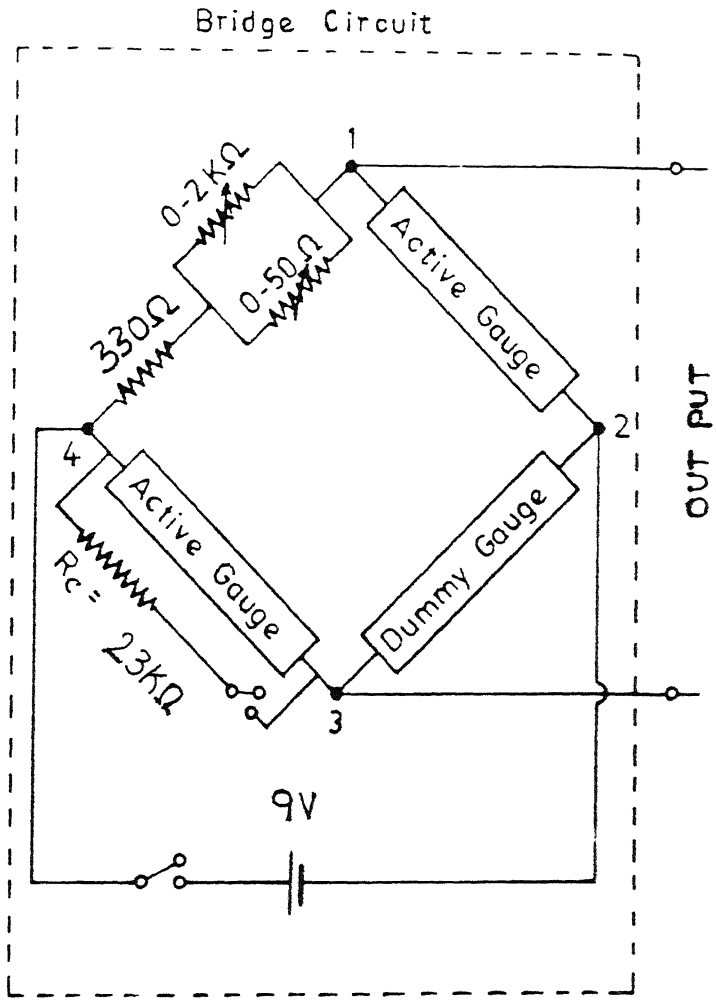

Fig. 4.5 Circuit of Wheatstone Bridge

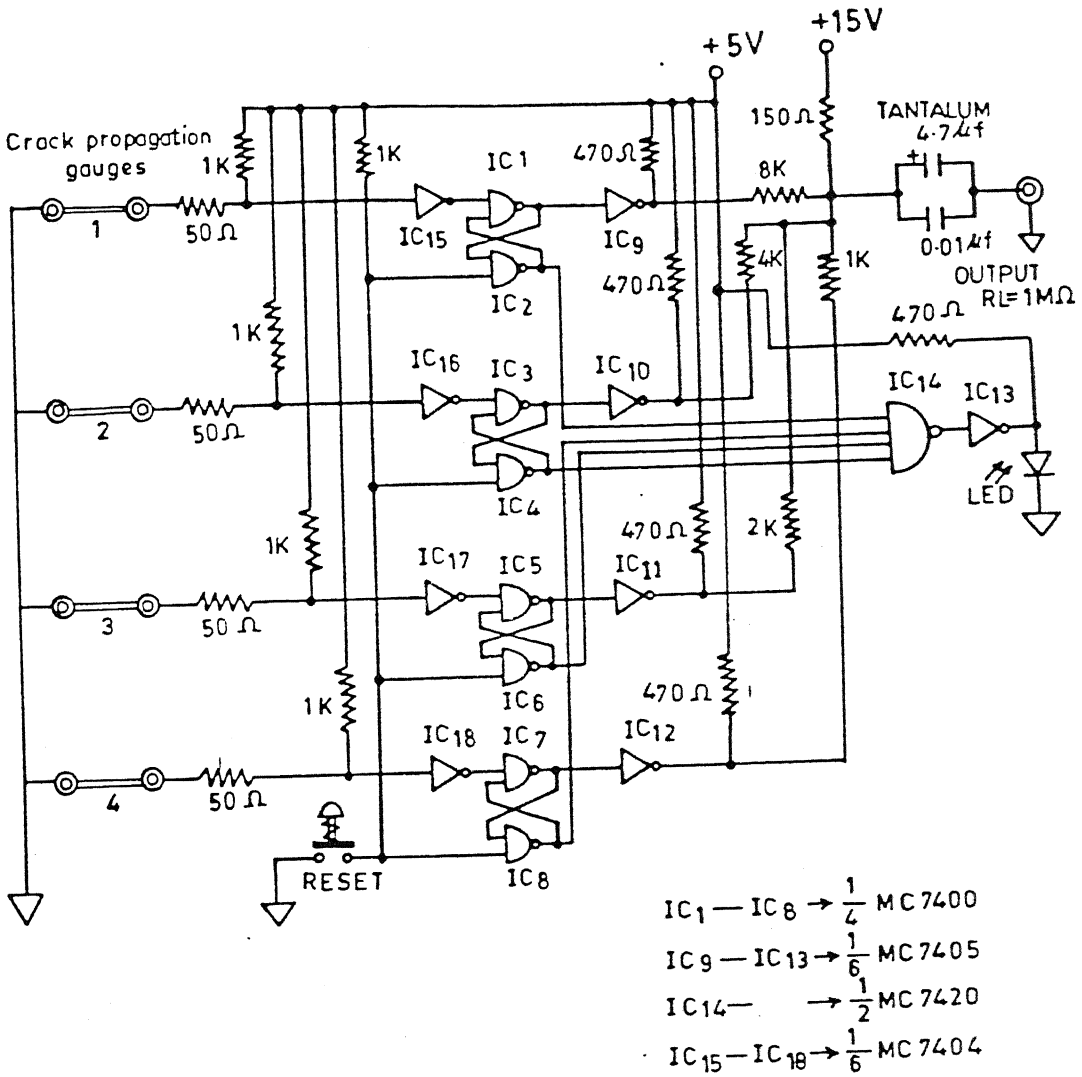

Fig. 4.6 Circuit of Logic Unit

ensures the continuity of the circuit. The circuit has been so designed that the successive potential drops occur in the output of the circuit due to the snapping of the four propagation gauges. The four drops appear as four steps in a stepped wave form against a time scale in the oscilloscope trace. The time duration between each drop and the distance between each adjacent gauge gives the crack velocity over a distance of about 2 mm in front of the crack tip. The top view of the specimen after bending is shown in figure 4.7 . Another view showing the position of the specimen is given in figure 4.8 .

4.8 Caliberation of the Bridge Circuit :

For the measurement of the loads on the specimen, the bridge circuit was caliberated before conducting the experiment. The bridge is balanced using the 50Ω and 2KΩ variable resistors. The caliberation resistance R_c is included in the circuit using a switch which shows a voltage deflection on the oscilloscope . The value corresponds to the strain of the bridge-strain gauge circuit. The caliberation strain is given by[17]

$$\varepsilon = \frac{2R_g}{S_g (R_g + R_c)} \qquad (4.11)$$

where R_g is the gauge resistance

and S_g is the gauge factor

Hence the strain recorded by the oscilloscope corresponding to 1mv deflection is obtained. The load on the specimen is calculated from the strain record.

Fig. 4.7 Top View of the Specimen after Impact

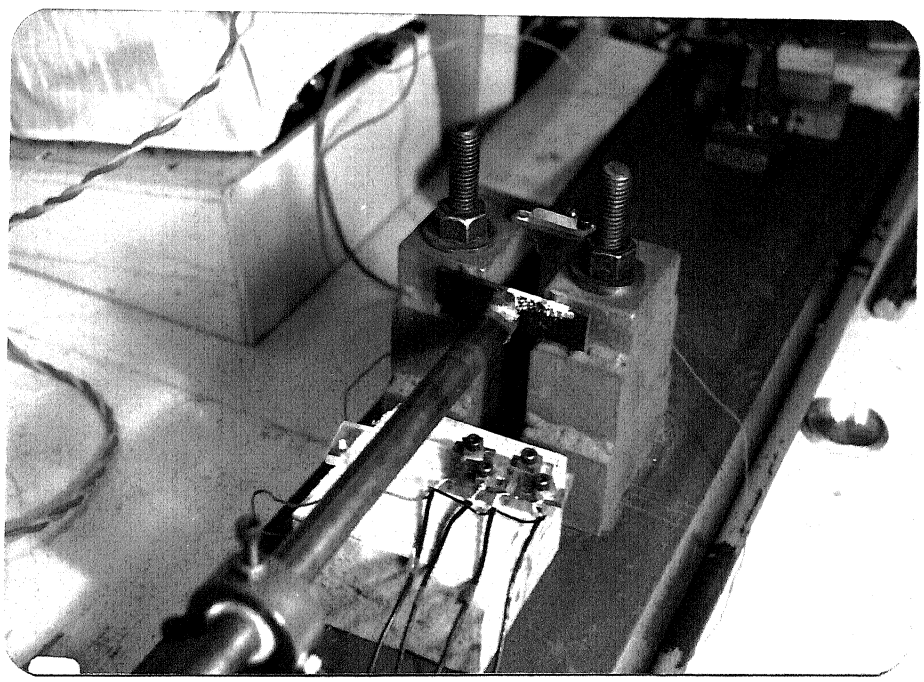

Fig. 4.8 Another view of the Specimen in 3-point Bending

CHAPTER 5

RESULTS AND DISCUSSIONS

5.1 Analysis of Stress Pulse Records :

A technique has been developed to determine the critical energy release rate values in mode II (G^{D}_{IIC}) under dynamic conditions. In this study, the technique was applied to Carbon/Epoxy composites. The impact of the striker with the load bar generates one dimensional stress waves. These waves are sensed by the strain gauges and recorded by the oscilloscope. A typical stress wave form is shown in figure 5.1 . The incident pulse shows a rise time of 17.8 μs while the reflected pulse takes a longer rise time of 23.7 μs. Following the relations of equation 4.7 and 4.8, the loads and the particle velocities at the end of the load bar are found. A set of graphs showing the variation of the load versus time and particle velocity versus time is given in figures 5.2 and 5.3 respectively. The load increases to a value of 16.49 kN in 12 μs and drops to zero in 31 μs. It is noted that the load time graph shows a peak. The particle velocity increases to a value of 5.5 m/s in 33 μs and remains constant. The load bar loads the specimen in 3-point bending. The work done on the specimen is used to increase the strain energy and the kinetic energy of the specimen and to form new surfaces. The work done or the energy input to the specimen varies with time which is shown in figure 5.4. The amount of work input reaches a maximum value of 0.05 joules in 18.5 μs.

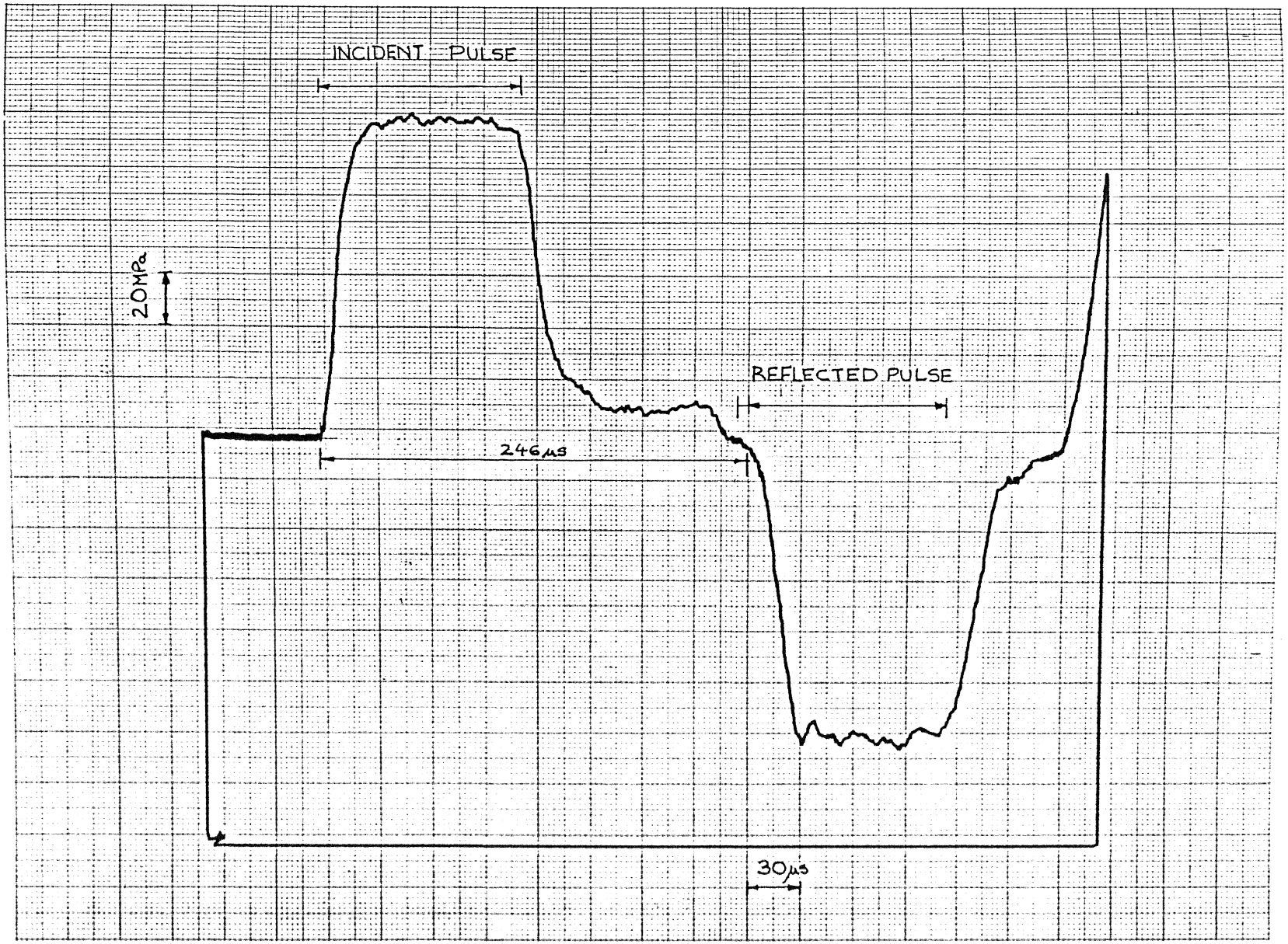

Fig. 5.1 A Typical stress Waveform Showing the Incident and Reflected Pulses

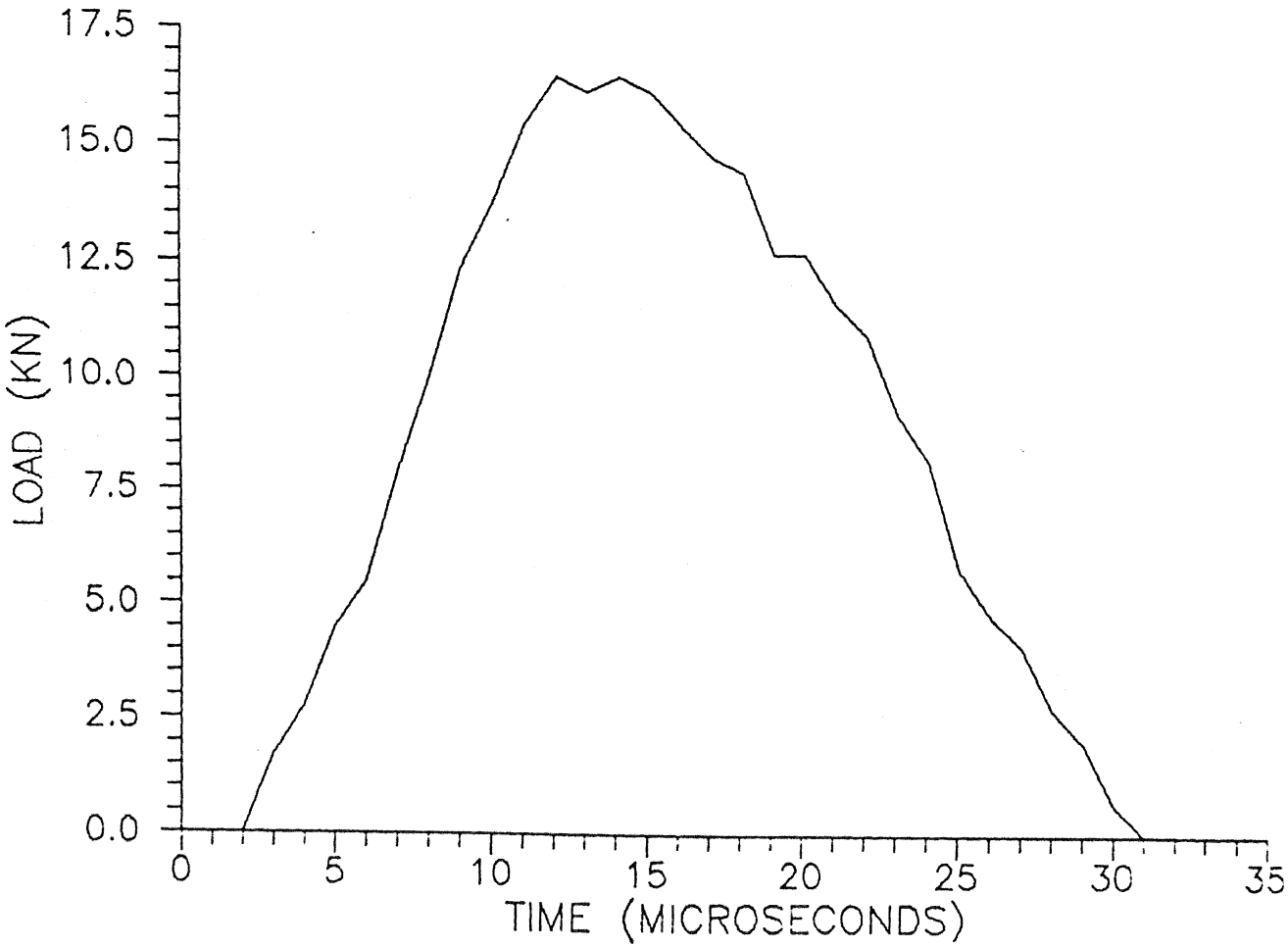

Fig. 5.2 Load - Time (P-t) Relationship

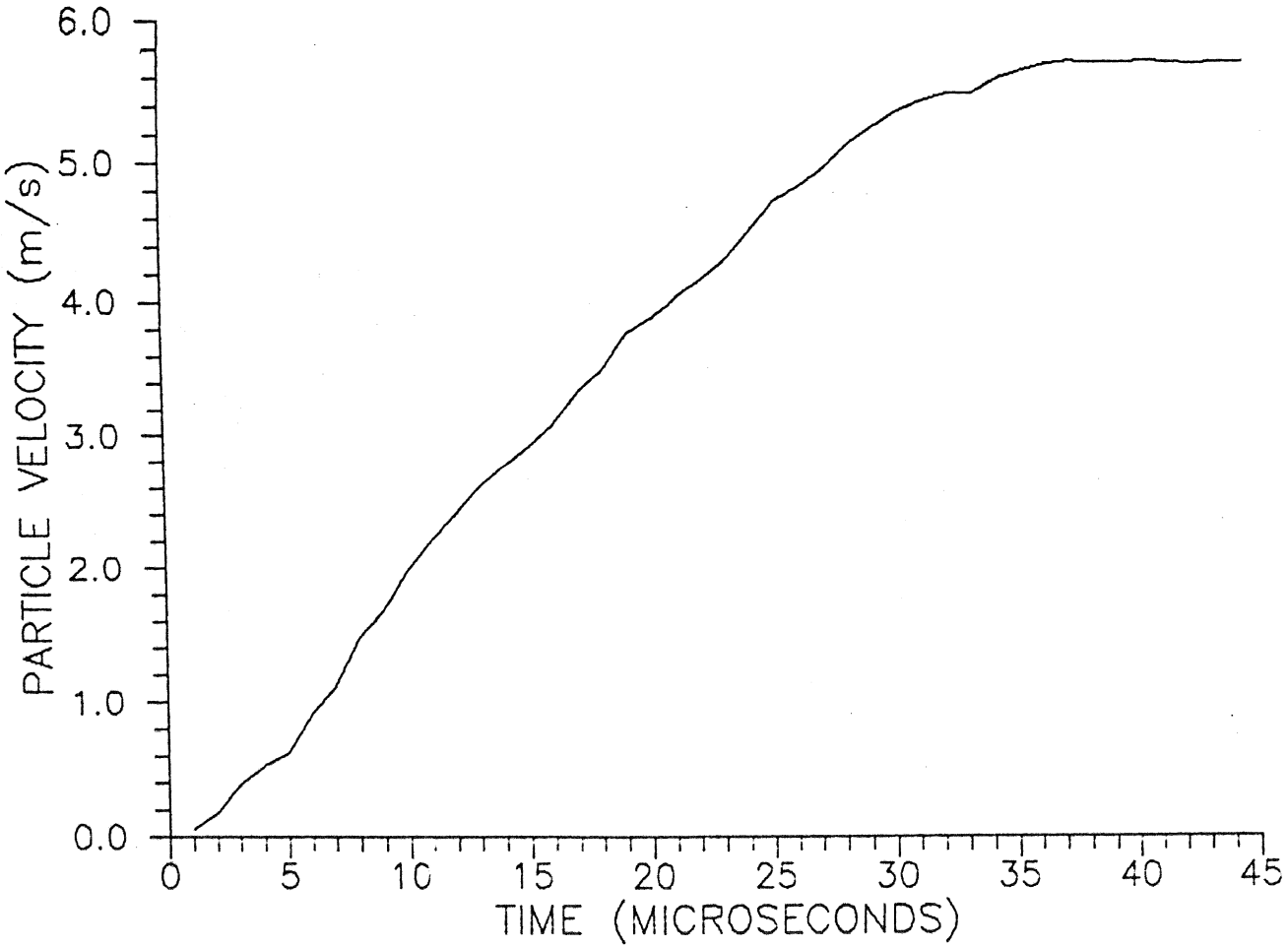

Fig. 5.3 Particle Velocity – Time (V-t) Relationship

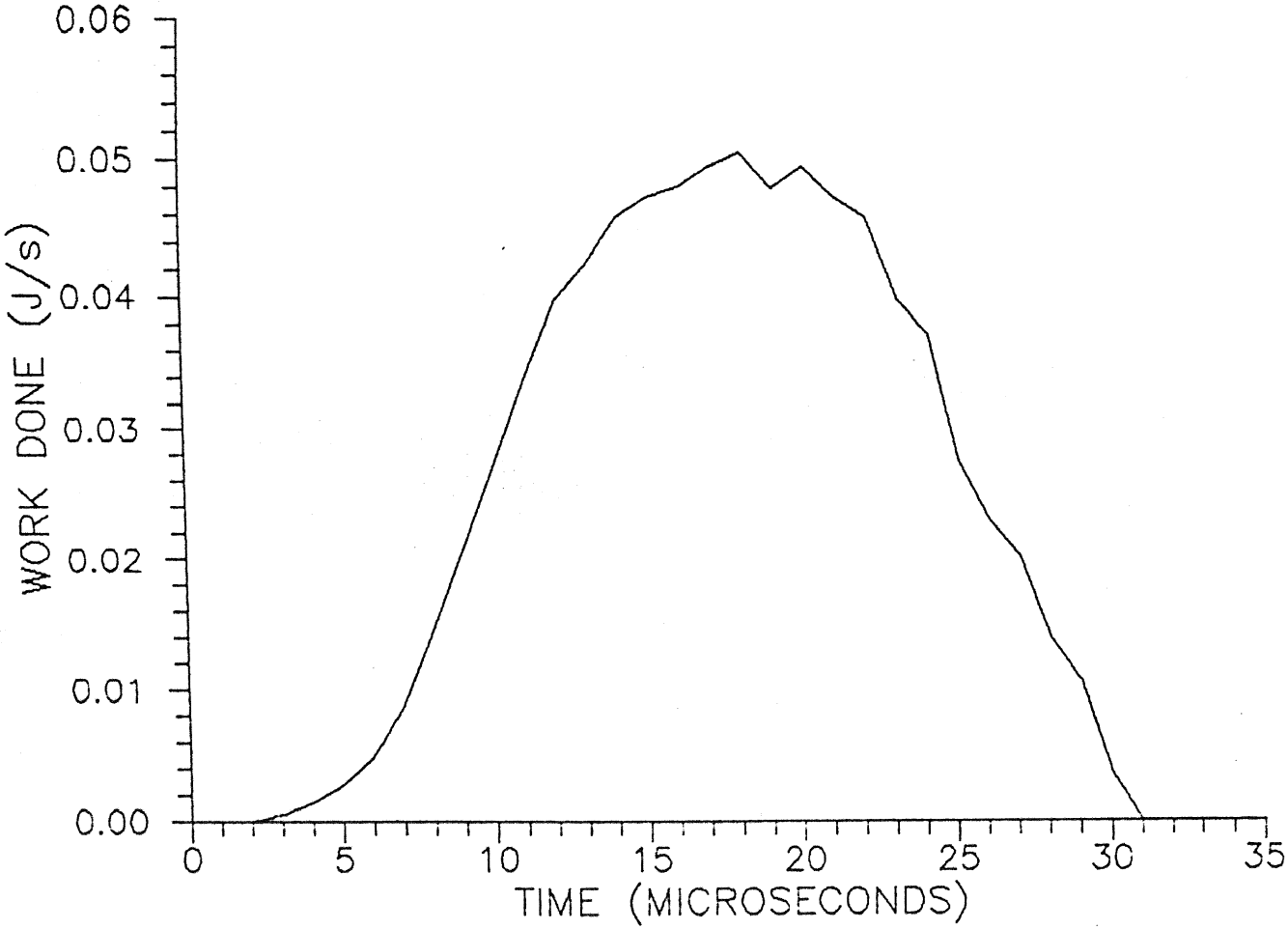

Fig. 5.4 Work done - Time (W-t) Relationship

5.2 Conditions for Crack Propagation :

Separate experiments were conducted to examine the behaviour of the pulses to the presence of cracks and different boundary conditions. The following cases were considered :

(a) Specimen with no crack and no supports

(b) Specimen with a crack and no supports

(c) Specimen with no crack and with supports

(d) Specimen with a crack and with supports

The geometry of the supports was not varied in the above cases. The incident and reflected pulses in each case are shown in figure 5.5 . The superposition of the reflected pulse over the incident pulse (figure 5.6) shows the difference in rise times; and the load on the specimen at an instant is proportional to the difference in the magnitudes of the pulses.

In the specimen with no crack and no supports, the incident and reflected pulses almost coincided with each other if the attention is confined to the rise time only. The slight difference in the stress value loads the specimen to the peak value of 1.42 kN (figure 5.7). The specimen with crack and no supports shows the incident and reflected pulses coinciding with each other during the rise time. The load on the specimen was zero. As expected, the crack in the specimen did not propagate. In the third case the reflected pulse of the specimen without crack and with supports had a smaller slope than that of the incident pulse. The load time graph shows a peak of 7.35kN(figure 5.7). In the fourth case of the specimen with crack and with supports the rise time is more for the reflected pulse in comparison to the incident pulse. From the difference, the load on the specimen is evaluated as shown in figure 5.7 .

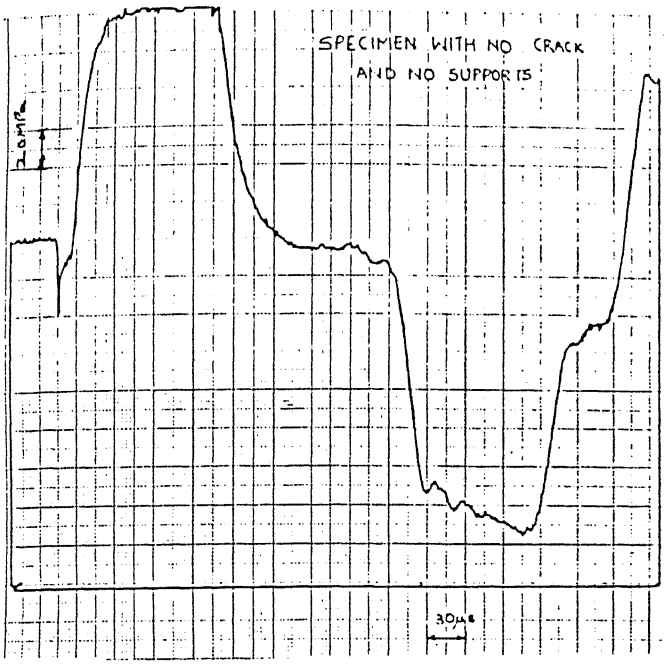

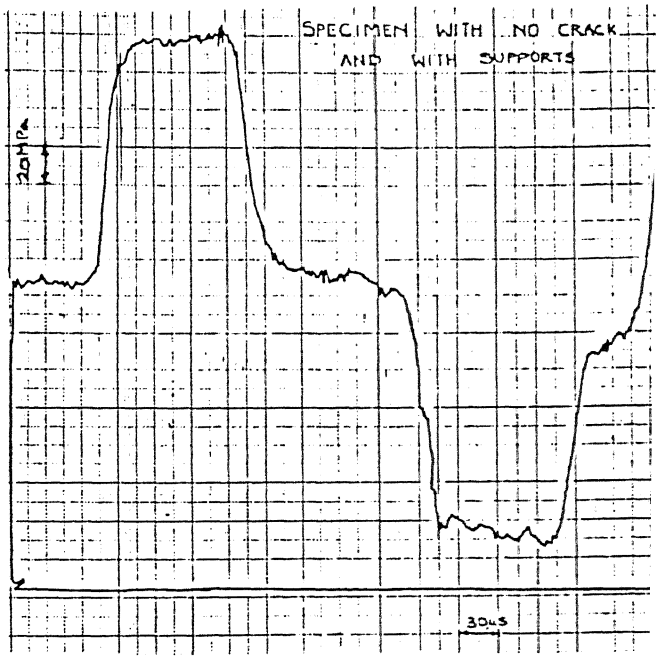

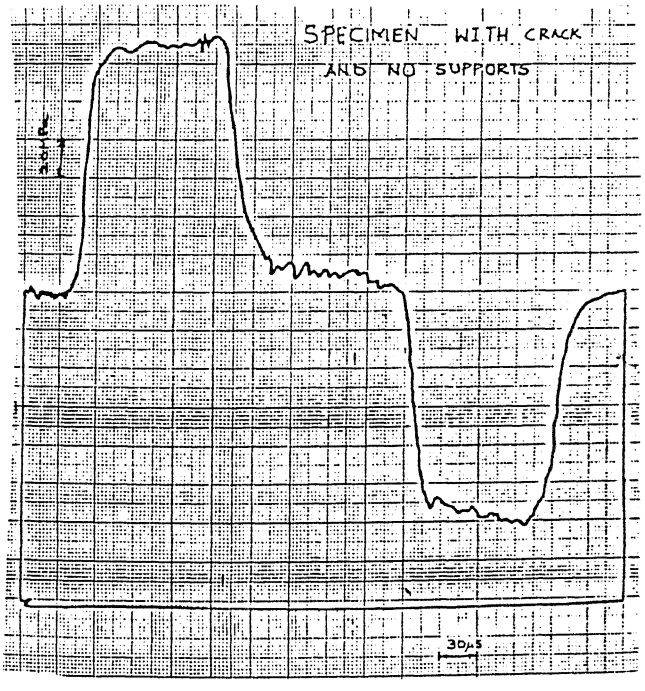

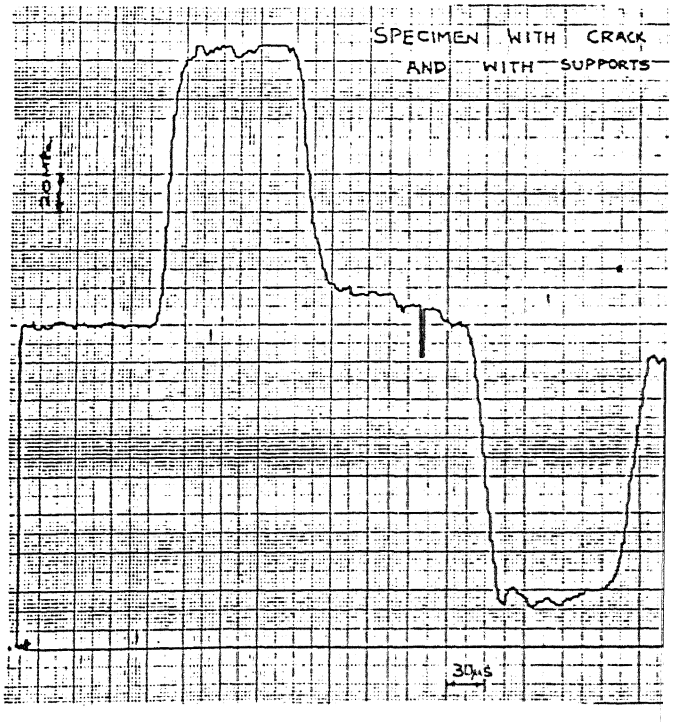

Fig. 5.5 Incident and Reflected Pulses to Examine the Behaviour of Stress Waves

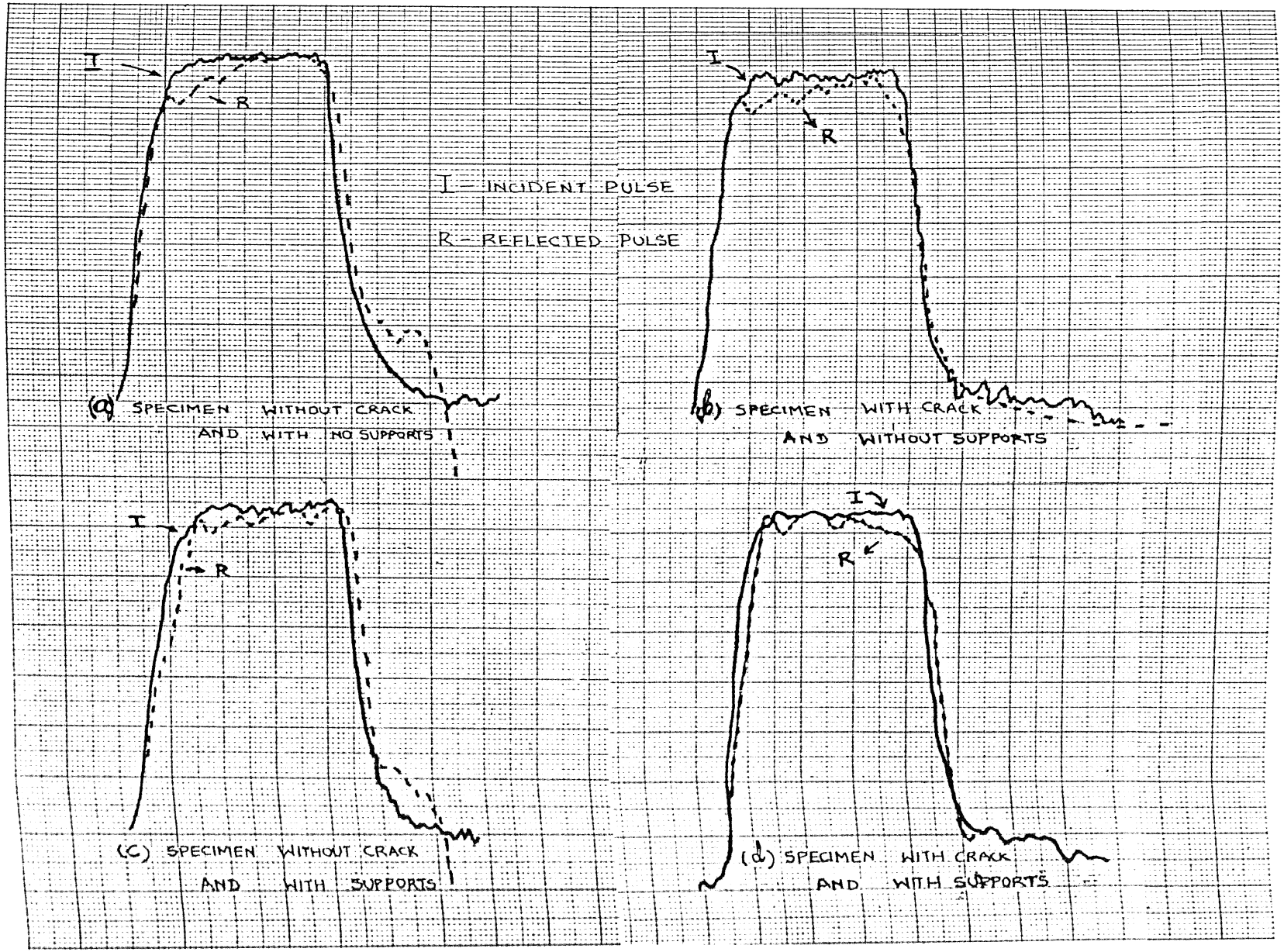

Fig. 5.6 Superposition of Incident and Refleted Pulses

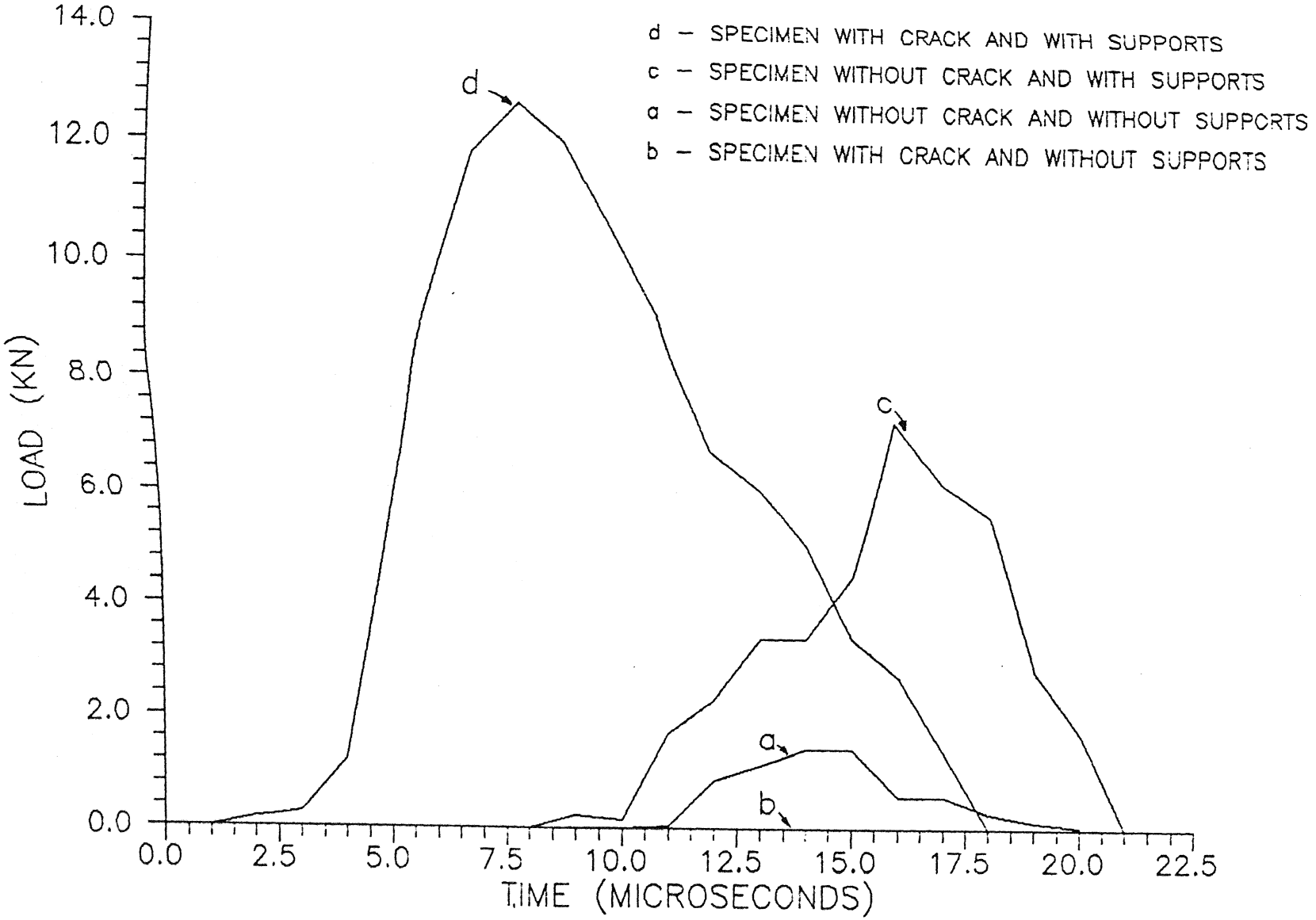

Fig. 5.7 Load - Time (P-t) Relationship for the Four Cases.

The load vs time relations of cases (d) and (c) correspond to specimens with and without crack respectively. The presence of the crack makes the peak load occur earlier. This suggests that the crack had started to move which decreased the specimen stiffness and hence the load on the specimen. All the four cases show that the rise time should be the focus for crack propagation studies.

5.3 Data Reduction

The analytical strain energy release rate formulation in an elastic body is based on the energy balance that includes the kinetic energy, K. Expressed in terms of compliance, the dynamic strain energy release rate for the onset of crack propagation is given by

$$G^{D}_{IIC} = \frac{P^{2}}{2W} \frac{dC}{da} - \frac{1}{W} \frac{dK}{da} \qquad (5.1)$$

where P is the applied load in a three point bend specimen, C is the specimen compliance, W is the specimen width and a is the crack length.

For a linear elastic body

$$\delta = C P \qquad (5.2)$$

where δ is the deflection under the load.

At the peak of load vs time graph of figure 5.2, the load does not vary with the extending crack.

Differentiation of equation 5.2 gives

$$\frac{dC}{da} = \frac{1}{P_c} \frac{d\delta}{da} \qquad (5.3)$$

where P_c is the peak load.

Substituting in equation 5.1 one obtains

$$G^{D}_{IIC} = \frac{P}{2b} \frac{d\delta}{da} - \frac{dK}{bda} \qquad (5.4)$$

Considering the rate of specimen deflection and crack growth the above equation reduces to

$$G^{D}_{IIC} = \frac{P_c}{2b} \frac{d\delta/dt}{da/dt} - \frac{dK}{bda}$$

$$= \frac{P_c V}{2 b \dot{a}} - \frac{dK}{bda}$$

where V is the velocity of the specimen under the load bar and $\dot{a}$ is the crack propagation velocity. The velocity V is taken from figure 5.2 corresponding to the time which shows the peak load in figure 5.1

In order to evaluate the second term in equation 5.5, the 3-point bending can be considered as two cantilevers loaded on either side of the centre as shown in figure 5.8.

dynamically at the centre under the load bar and thus acquires kinetic energy. The second term of equation 5.5 accounts for the change in kinetic energy. The deflection of the left half of the beam (figure 5.8) is given by

$$\delta = \frac{P_c}{12EI} (- X^3 + 3LX^2) \qquad 0 < x < L \qquad (5.6)$$

The maximum deflection of the beam is

$$\delta_{max} = \frac{P_c L^3}{6EI} \qquad (5.7)$$

Normalising equation 5.6 with δ_{max} ,one obtains

$$\frac{\delta}{\delta_{max}} = \frac{(-X^3 + 3LX^2)}{2L^3} \qquad 0 < x < L \qquad (5.8)$$

For making an estimate of the kinetic energy, the change in the stiffness due to the presence of crack has not been accounted for. This does not make an appreciable difference in the results as the first term in equation 5.5 was found to dominate.

Considering the velocity variation to be similar to that of the deflection

$$\frac{v_b}{v_b} = \frac{(-X^3 + 3LX^2)}{2L^3} \qquad 0 < X < L \qquad (5.9)$$

where v_b is the velocity at point X.

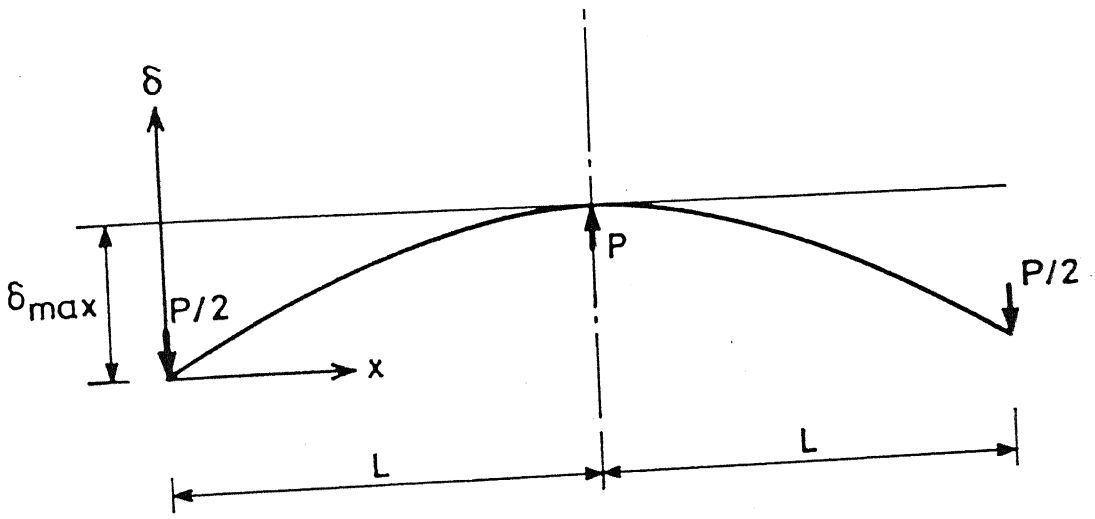

Fig.5.8 3-point bending of specimen.

ergy of the left half of the beam is given by

$$K_L = \int_0^L \frac{1}{2} (\rho dx)\, v_b^2$$

$$= \rho \int_0^L \frac{(-x^3 + 3Lx^2)^2}{4L^6} V_b^2\, dx$$

$$= \frac{33}{280} \rho V_b^2 L \qquad (5.10)$$

The kinetic energy of the right half of the beam is same as e left half, and so the kinetic energy of the entire beam is

$$K = \frac{33}{140} \rho V_b^2 L$$

The kinetic energy term associated with the critical energy elease rate is given by

$$\frac{dK}{bda} = \frac{33}{70} \frac{\rho L V_b}{b} \frac{dV_b}{da}$$

$$= \frac{33}{70} \frac{\rho L V_b}{b} \frac{\dot{V}_b}{\dot{a}} \qquad (5.11)$$

Substituting equations 5.11 in equation 5.5 the relation for he dynamic critical energy release rate is

$$G^D_{IIC} = \frac{1}{2b\dot{a}} \left[P_c V - \frac{33}{35} \rho L V_b \dot{V}_b \right] \qquad (5.12)$$

5.4 Crack Velocity

The crack velocity or the rate of crack growth is determined

ending crack breaks the propagation gauges one after another. a result, the potential drops occurring in the logiccircuit are orded on the oscilloscope against a time scale as shown in figure . The logic circuit has been designed such that the first gauge a potential drop of 800 mV, the second 400 mV, the third 200 mV, the fourth 100 mV. Thus the potential drops indicate the order in ch the gauges have been broken. Also the time duration between the ops and the distance between the corresponding gauges determines the ack velocity. In most of the experiments the propagation gauges did break in proper sequence. The reasons for such a behaviour can due to reasons described as follows.

A large number of experiments were conducted to develop the chnique to obtain breakage of the gauges in sequence. The quence of breakage was found to be at random. Replacing the in copper wire (diameter 28 microns) by a slightly thicker wire iameter 60 microns) did not make any difference. The logic it was checked for the response time of each gauge. It was und to be smaller than the fastest time of two neighbouring cord points of the digital oscilloscope, that is, less than 0.5 .

It is now believed that the problem exists due to several actors. First of all the epoxy which is used to bond the gauges the specimen has much lower modulus than compared to .copper. onsequently the cracked two halves of the epoxy do not work as a ood shearing die. The epoxy under the sideways force of the wire s compressed rather than cutting the wire. Also, the thin wire orks like a razor blade and to certain extent, cuts into the dges of the epoxy. As a result, the wire fails in tension in

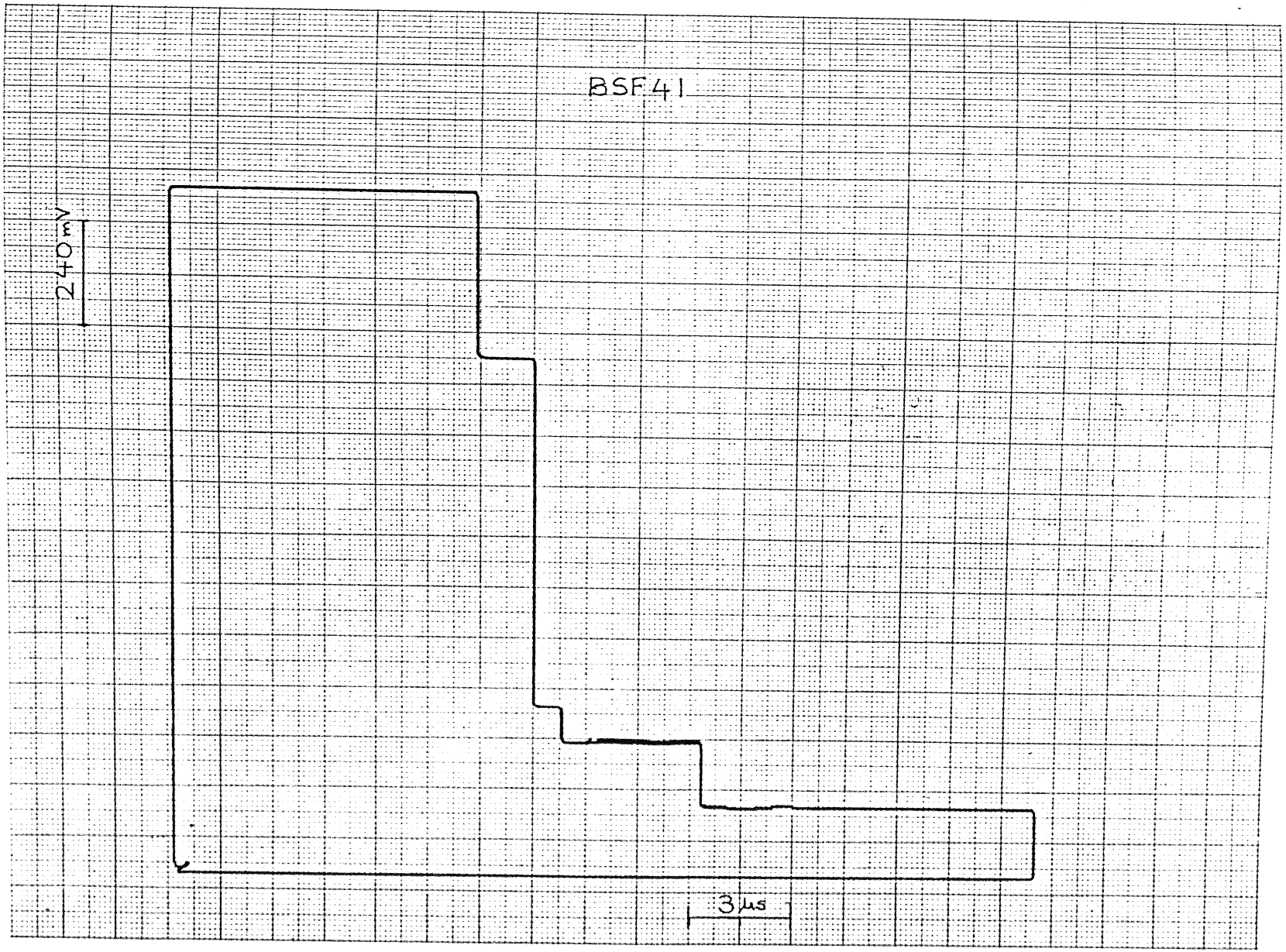

Fig. 5.9 An Oscillograph showing record of the Propagation Gauge Drops

with a scissor having a play between two blades. The wire tends to get elongated.

The breakage of wire in tension has its own problems. The copper wire used for the studying has a high ultimate strain of 14%. Each breakage would take a relatively long time in comparison to the time taken by the crack to move from one gauge to another.

Another problem is also associated with the breakage of wire in tension. The wires were bonded normal to the cracked faces. When one face slides over another with an unsupported or loosely supported wire in between the length of the wire,hardly changes its length (generally known as the cosine law). The wire would not break until a large amount of relative slide takes place. This makes the gauge less sensitive to each breakage.

These problems can be reduced considerably by proper choice of the gauge material such as replacing the copper wire by a carbon fiber with its low ultimate strain of about 1.5%. Also, the gauges can be bonded at an angle as shown in figure 5.10 ,to minimize the effect of cosine law.

These modifications could not be tried out due to the limitation of time. Hence the crack velocity was calculated by dividing the total distance between the recorded drops by the total time recorded by the drops.

5.5 Results

A number of experiments were conducted and their details are given in Table I. The width and thickness of the specimen were maintained around 20 mm and 4 mm respectively. Two

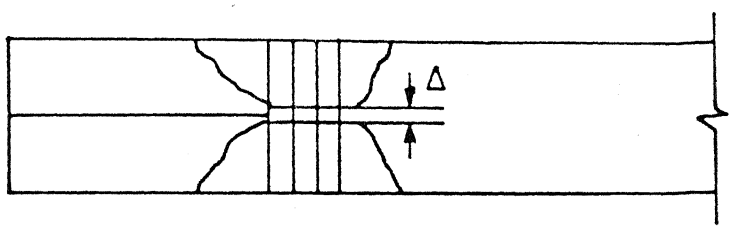

(a)

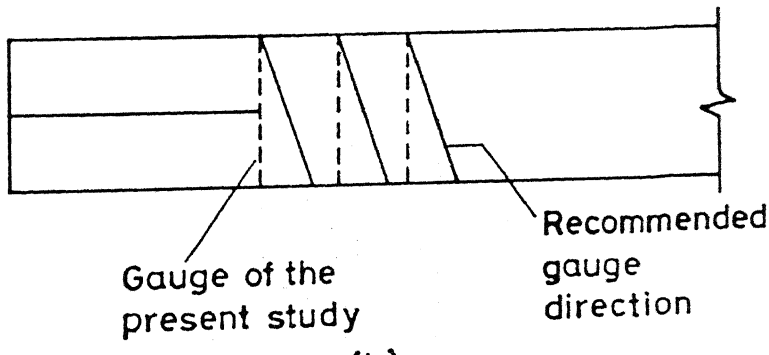

(b)

Fig.5.10(a) Gauge having free length Δ
(b) Suggested inclination of propagation gauges.

TABLE - I

EXPT. NO.	SHOT NO.	WIDTH (mm)	THICKNESS (mm)	SPAN (2L) (mm)	DIAMETER OF GAUGES (mm)	ORIENTATION CODE
1	BSF6	20.48	4.86	30.60	0.06	A
2	BSF24	20.06	3.52	30.60	0.06	B
3	BSF25	19.08	4.60	50.00	0.06	B
4	BSF26	18.00	4.62	50.00	0.06	B
5	BSF28	20.50	3.68	50.00	0.06	B
6	BSF33	20.72	3.96	50.00	0.028	C
7	BSF38	19.98	3.74	50.00	0.028	C
8	BSF39	20.04	4.00	50.00	0.028	C
9	BSF40	20.78	4.12	50.00	0.028	C
10	BSF41	19.98	3.78	50.00	0.028	C
11	BSF44	20.00	3.90	50.00	0.028	C
12	BSF47	20.34	3.76	50.00	0.028	C

A - [0/90/0/90/0/90/0/90/0/90/0/90/0/90/0/90/0/90/0]

B - [0/90/0/90/90/0/90/0/90/0/90/0/0/90/0/90]

C - [0/45/0/45/45/0/45/0/45/0/45/0/0/45/0/45]

length was increased from 30.6 mm to 50 mm to provide increased sliding between the cracked surfaces for from 60 μm to 28 μm to decrease the amount of energy spent in breaking the gauges. The orientation code (as given in Table I) was changed from A to B. This was done as the changed stacking sequence B has an interface with the symmetrical halves about the mid plane and the coupling stiffness matrix [B] is null. It was found that, in case B, the crack propagated on a different plane by breaking the fibres (weft) of the 90^{o} ply. Thus the code was again changed from B to C to facilitate the crack to propagate in its own plane as warp and weft are at 45^{o} to the crack propagating direction..

The wave-form records of twelve experiments are shown in figures (5.11 - 5.13). The nature of the incident and reflected pulses are almost identical except for BSF 6 (figure 5.11) which shows a peak before the rise time is over. The data obtained from these records are then processed to obtain the load (P) versus time (t) and particle velocity (V) versus time (t) plots. The plots are shown in figures (5.14 - 5.25). Most of the P-t plots show a sharp increase in load with a rise time of 12-16 μs, except for BSF44 and BSF47 which take 25μs and 20μs respectively. The load dies down in about 30μs in all other cases except BSF44 and BSF47 which take 42μs and 47μs respectively.The particle velocity rises almost linearly in most cases but for BSF 6 and BSF 33 which show a nonlinear rise. The particle velocity reaches a maximum value in all cases and remains constant.

The peak values of load and their corresponding particle velocities account for the change in the external work done per unit crack advance. As mentioned earlier, the crack velocities have been

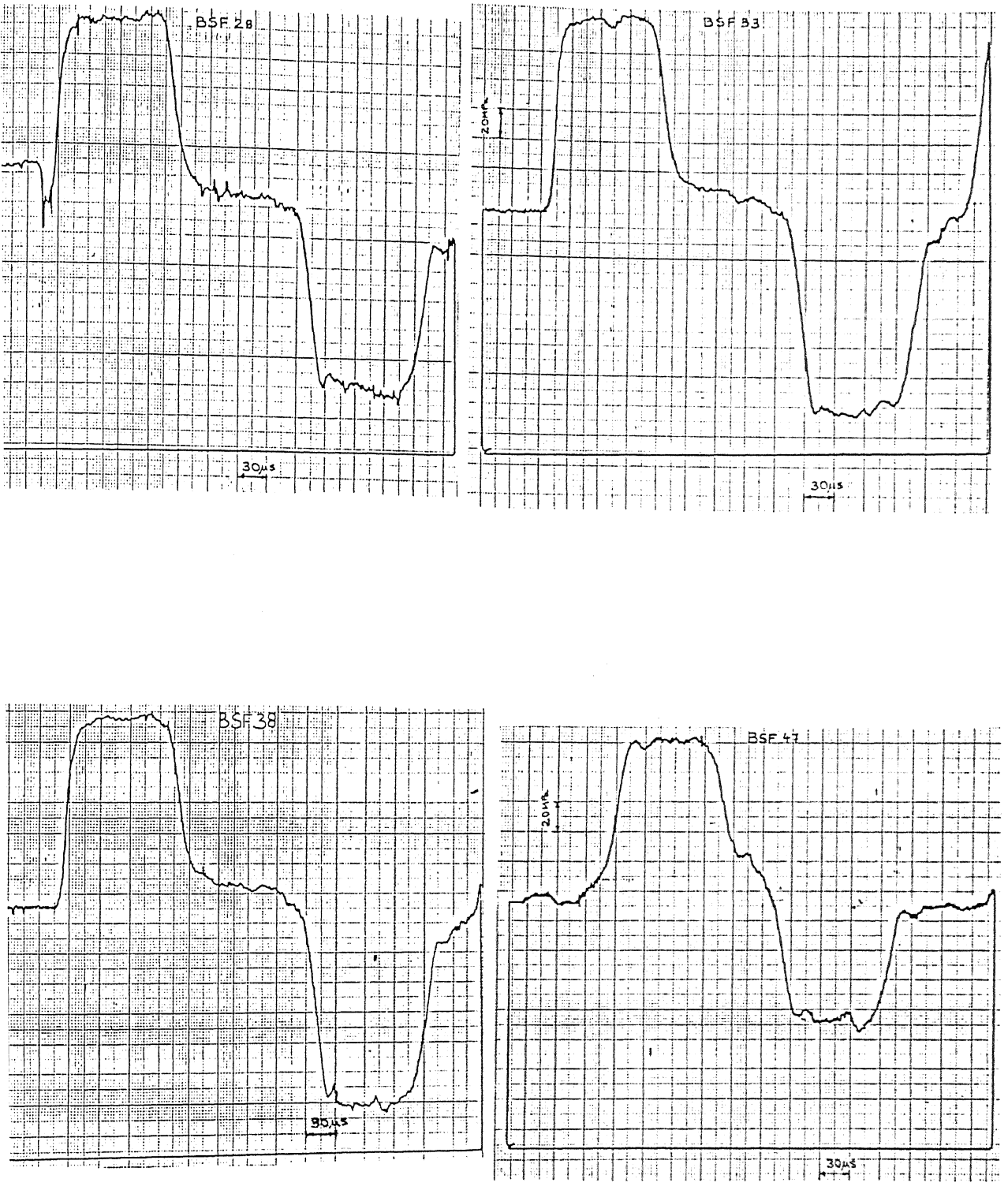

Fig. 5.12 Stress Pulses for Four Different Experiments

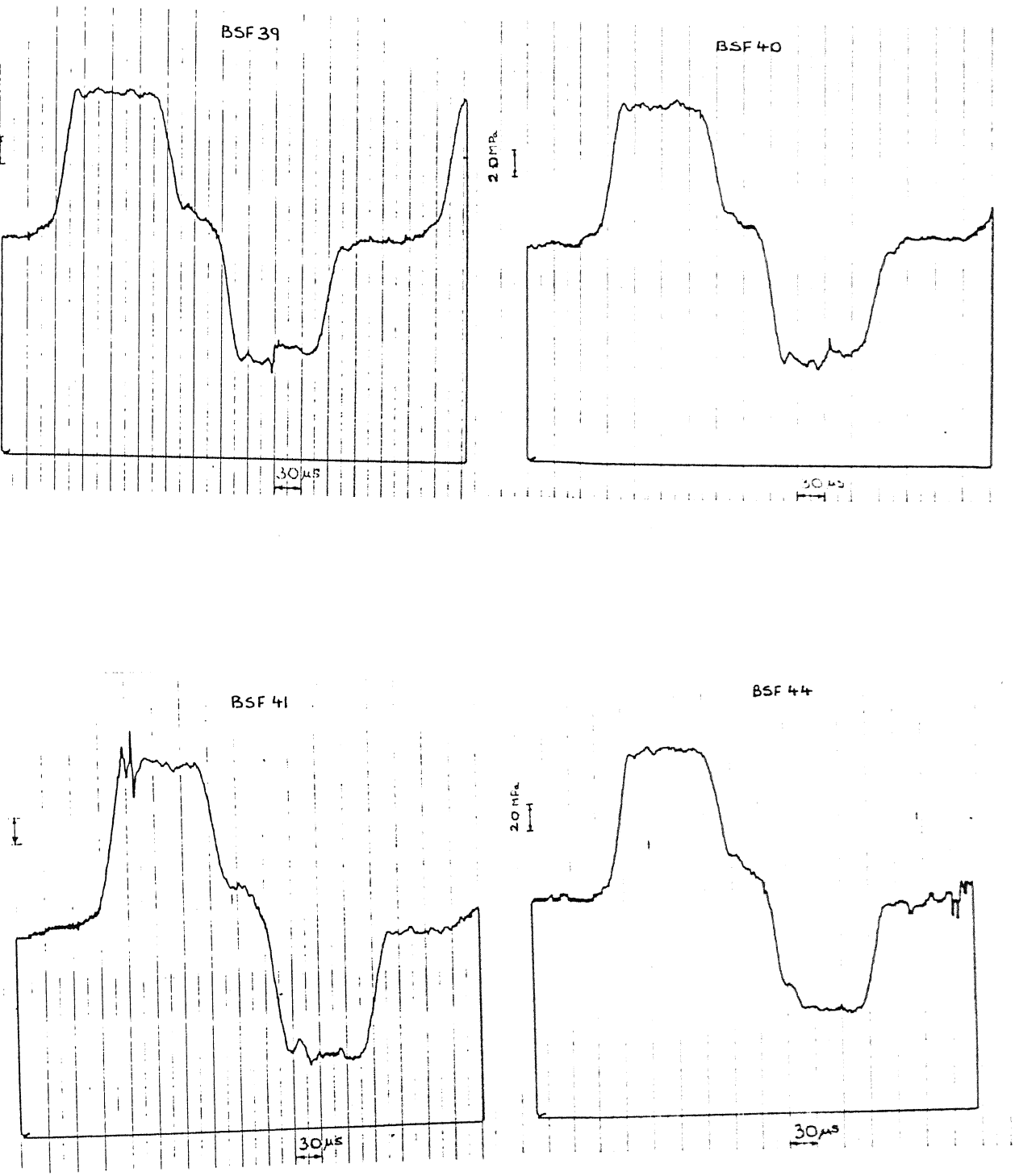

Fig. 5.13 Stress Pulses for Four Different Experiments

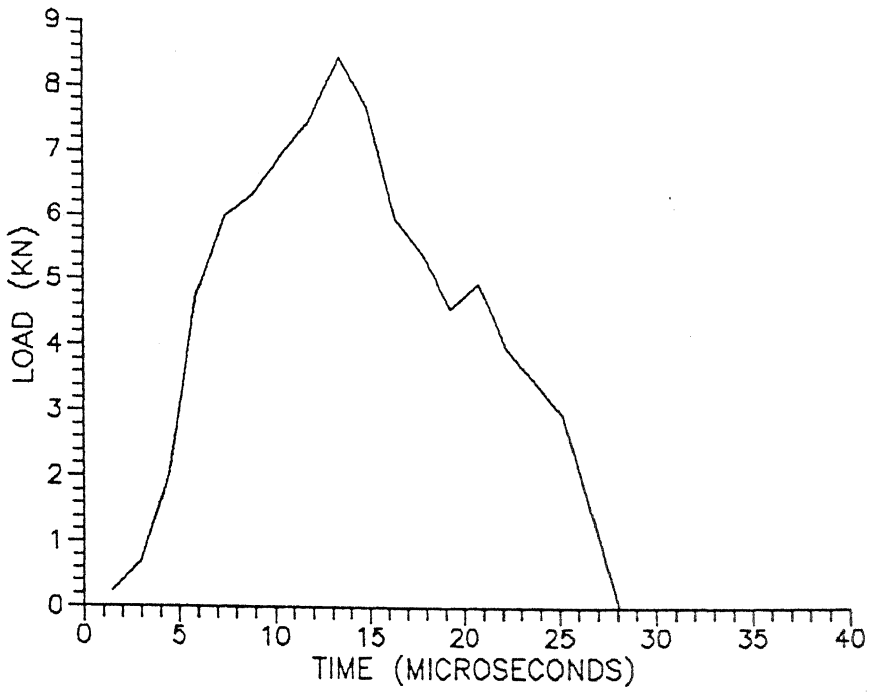

BSF24

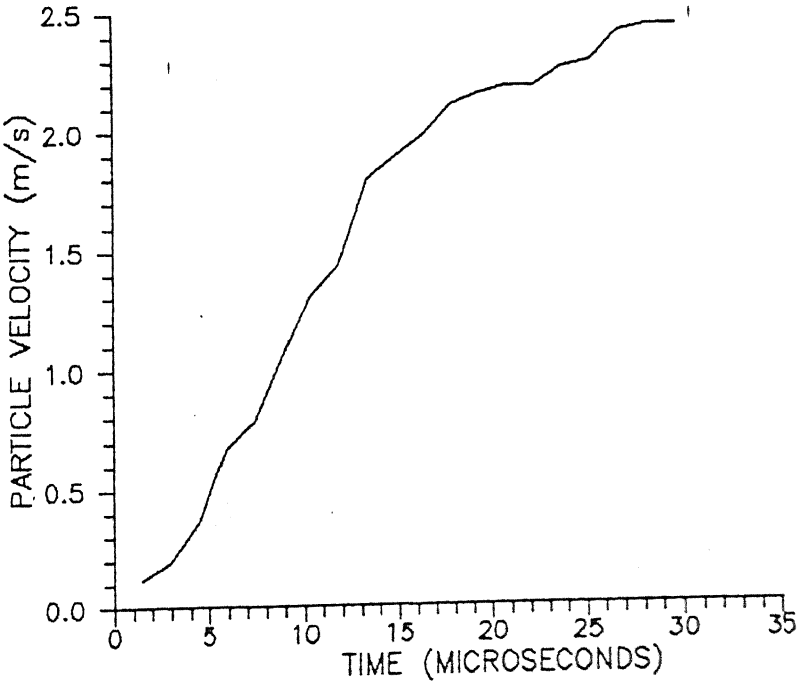

Fig. 5.15 (P-t) and (V-t) Relationship for Experiment BSF24

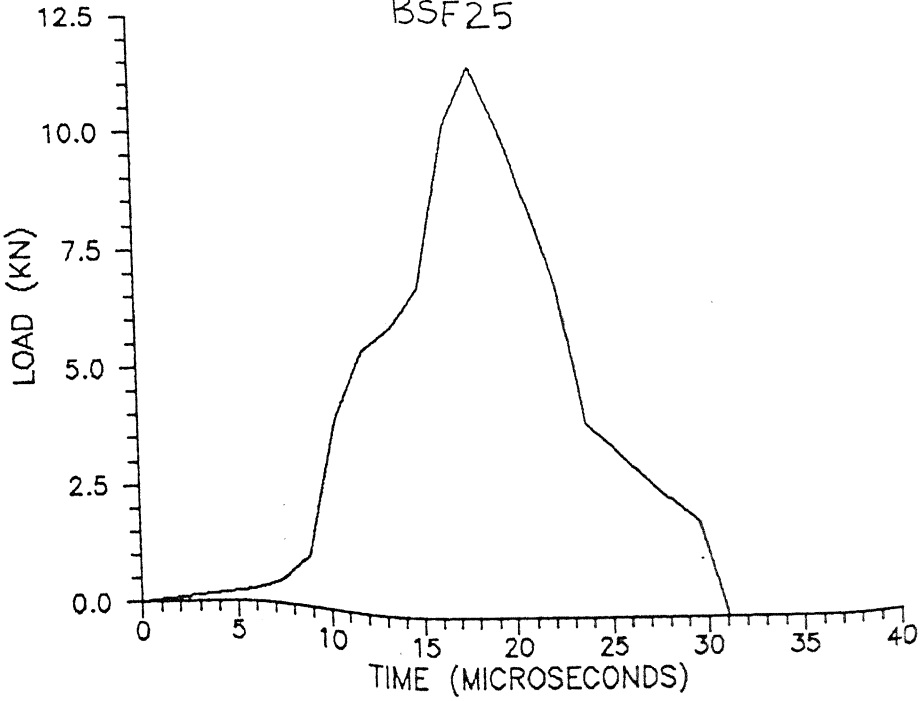

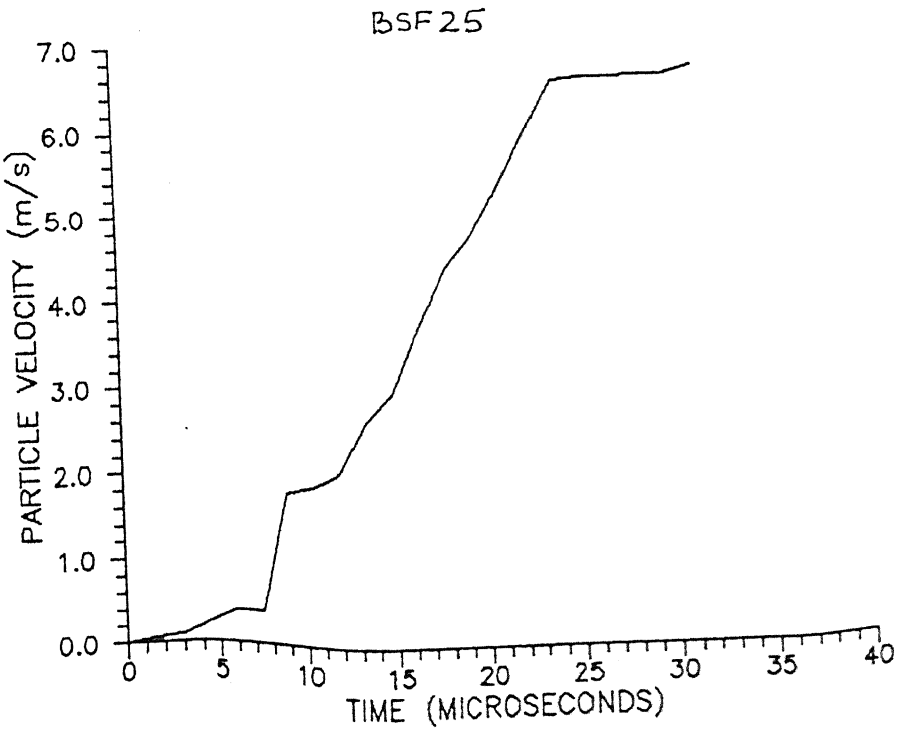

Fig. 5.16 (P-t) and (V-t) Relationship for Experiment BSF25

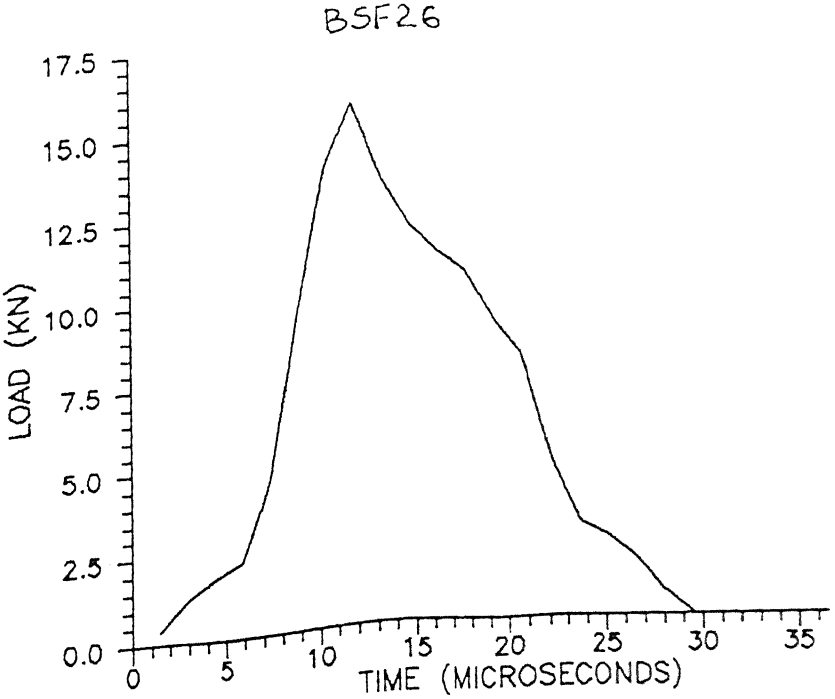

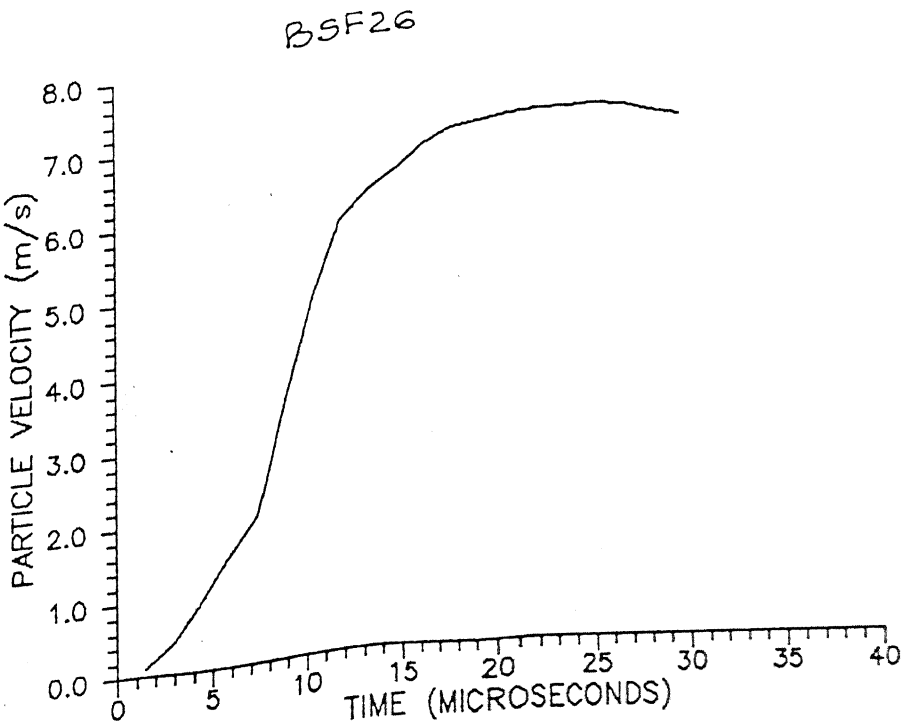

Fig. 5.17 (P-t) and (V-t) Relationship for Experiment BSF26

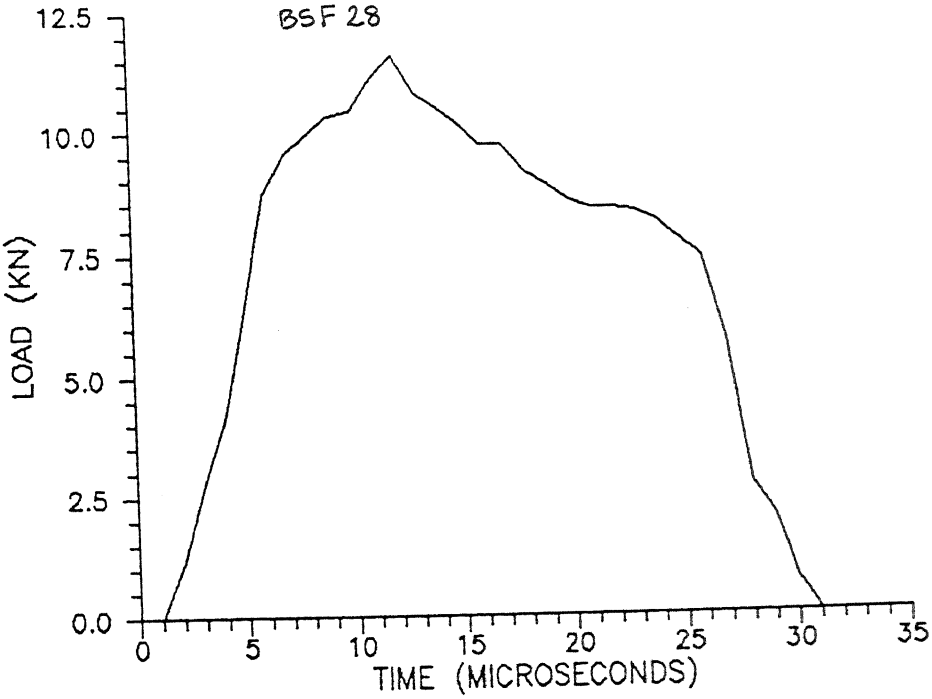

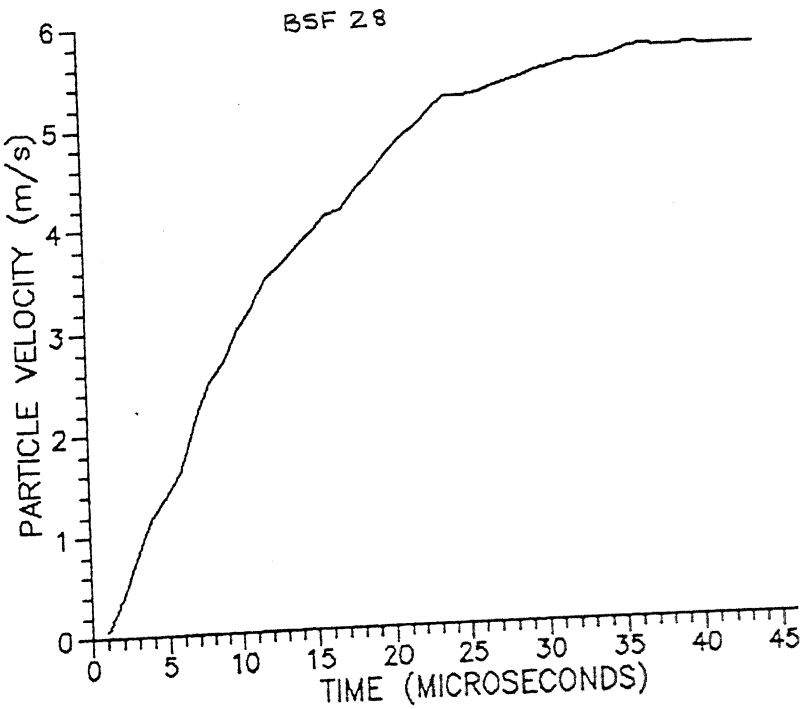

Fig. 5.18 (P-t) and (V-t) Relationship for Experiment BSF28

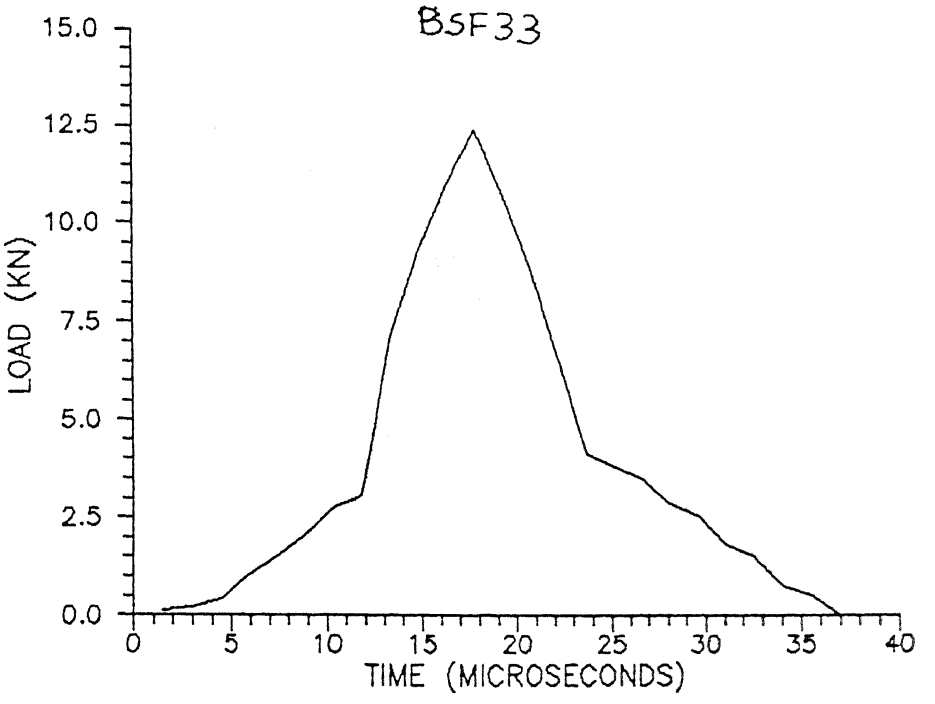

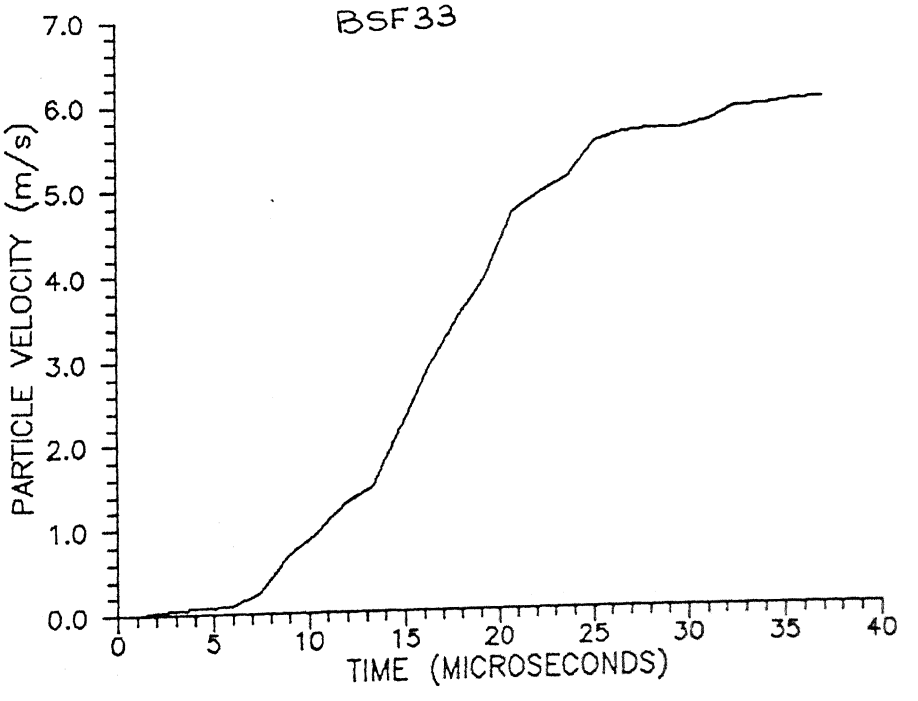

Fig. 5.19 (P-t) and (V-t) Relationship for Experiment BSF33

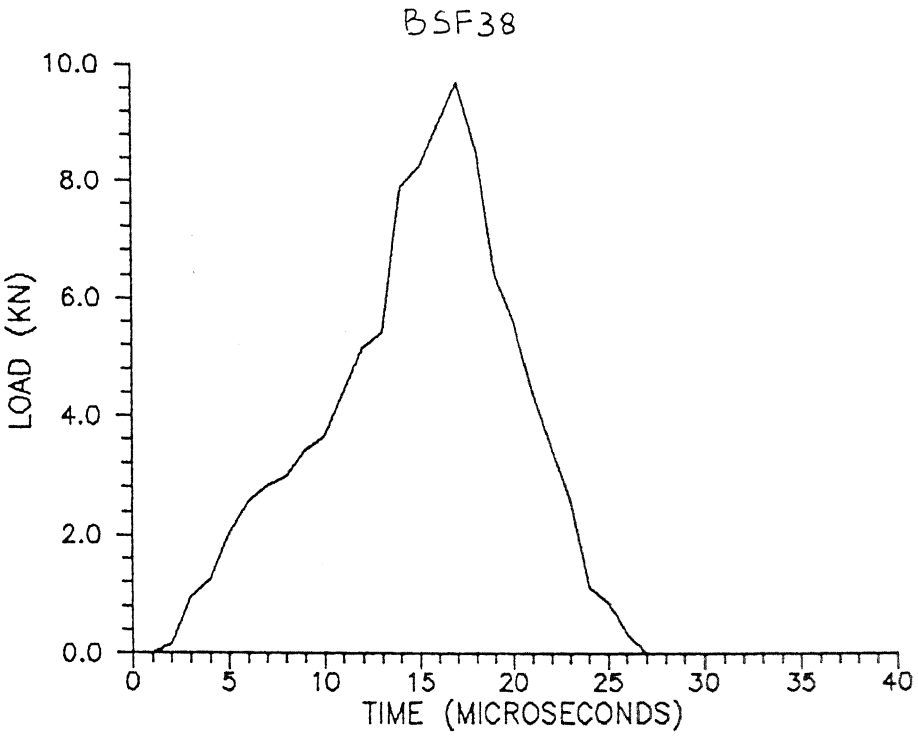

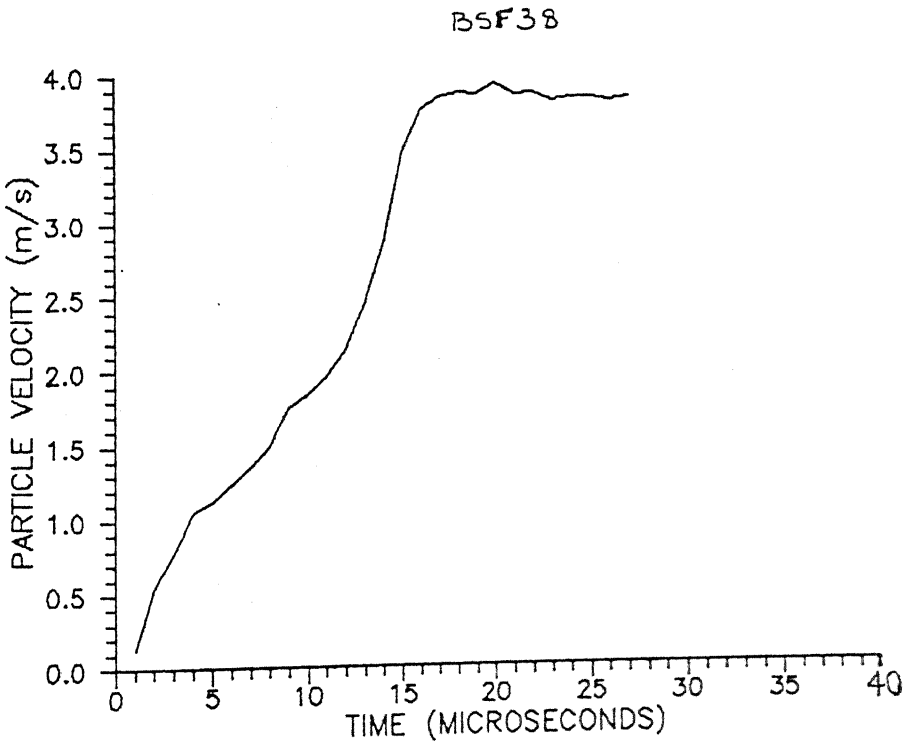

Fig. 5.2Ø (P-t) and (V-t) Relationship for Experiment BSF38

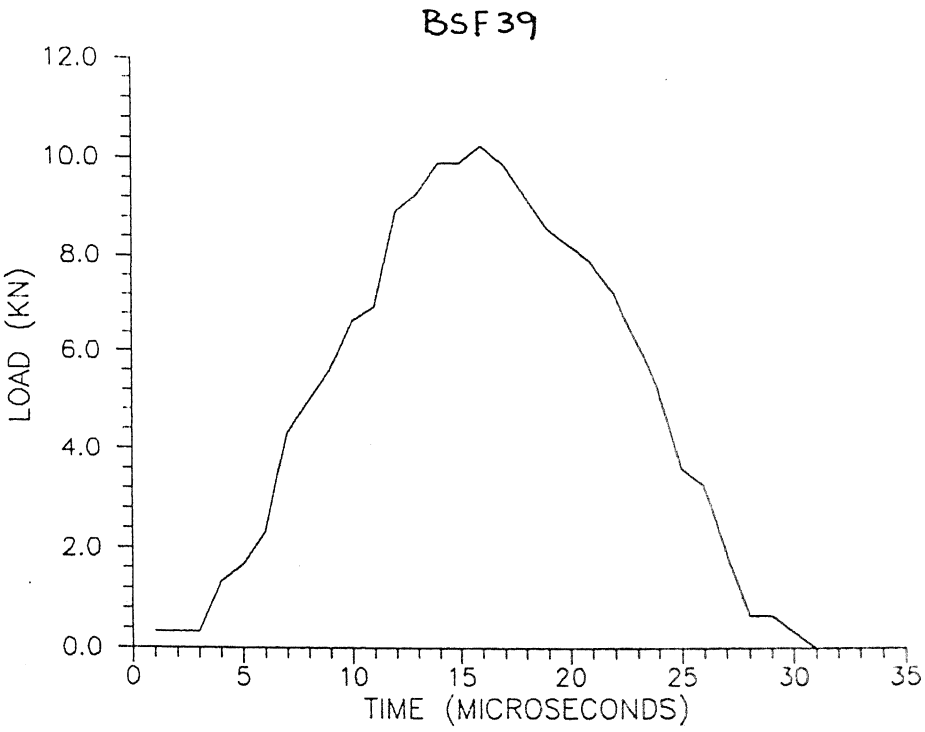

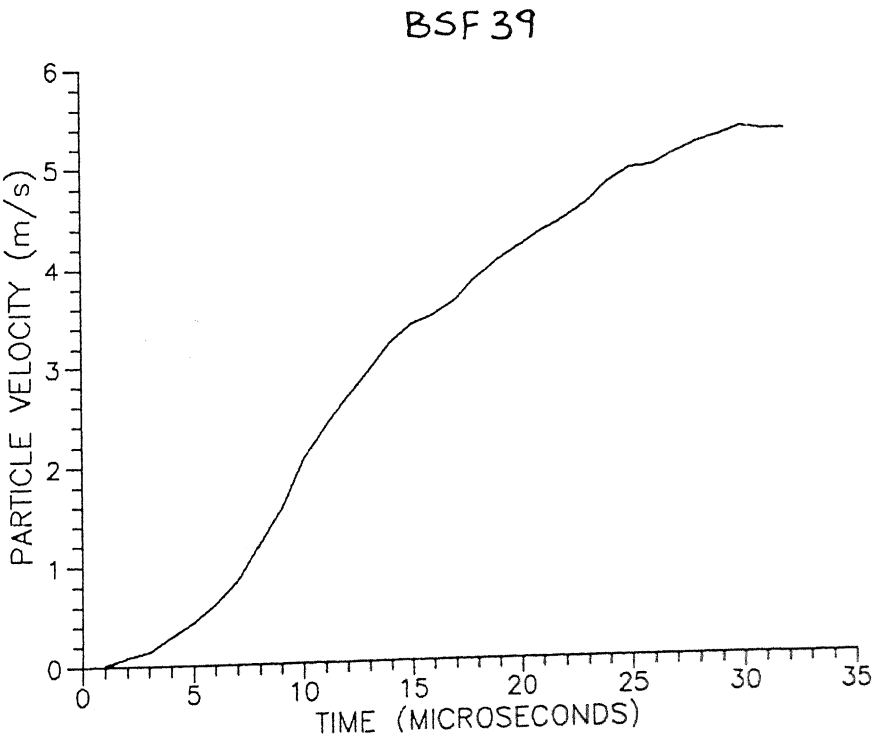

Fig. 5.21 (P-t) and (V-t) Relationship for Experiment BSF39

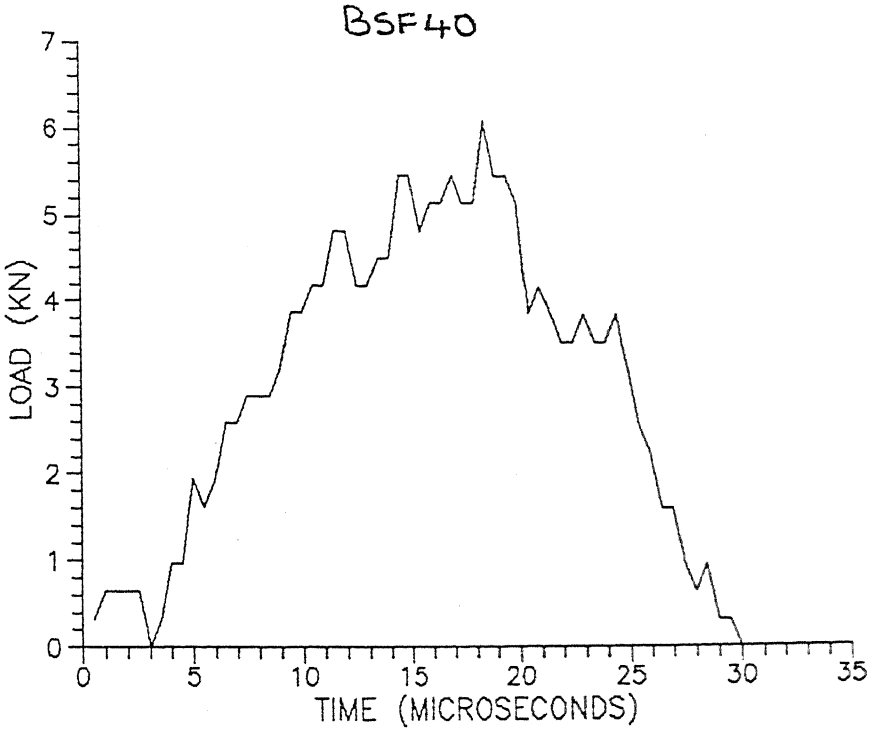

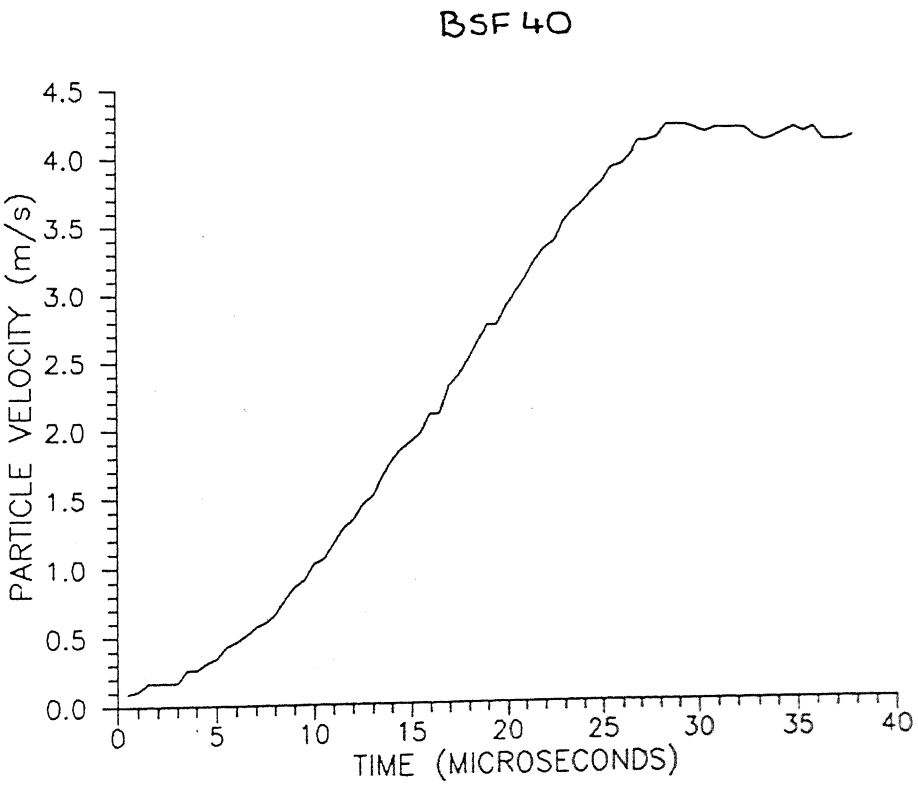

Fig. 5.22 (P-t) and (V-t) Relationship for Experiment BSF40

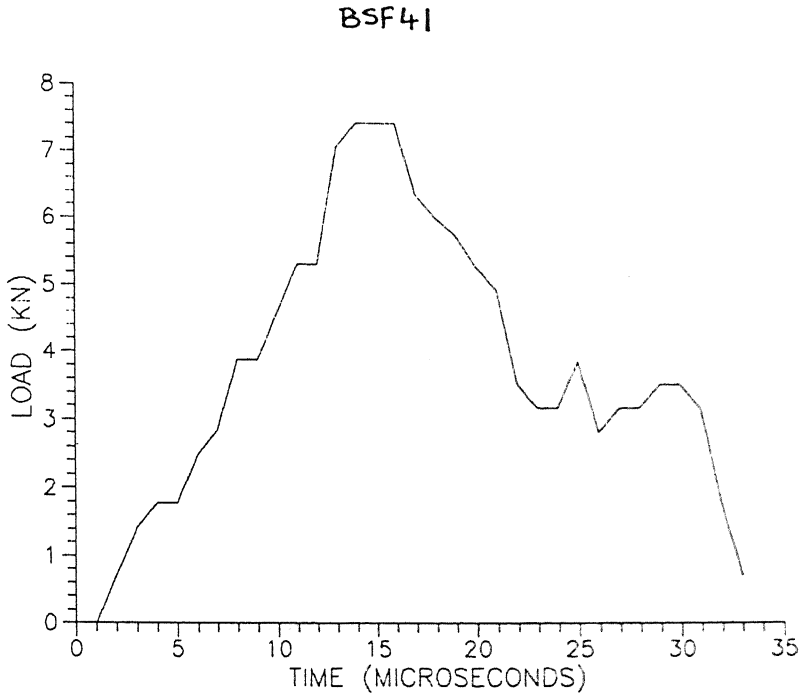

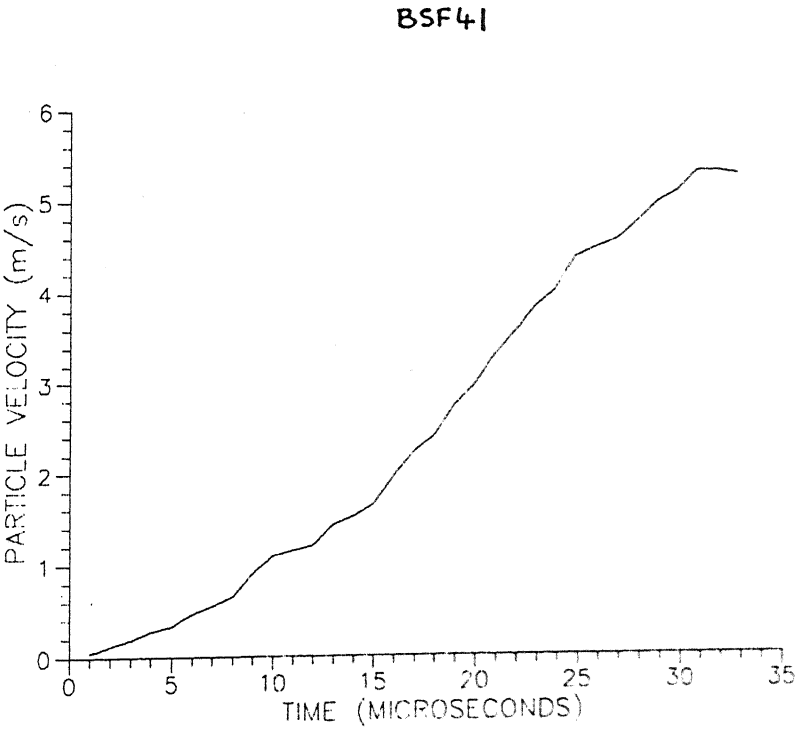

Fig. 5.23 (P-t) and (V-t) Relationship for Experiment BSF41

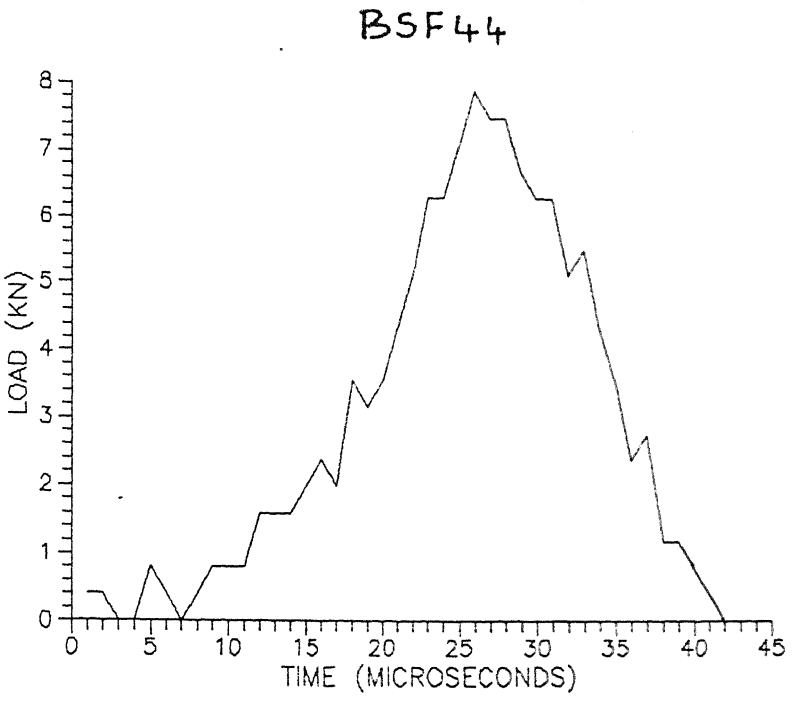

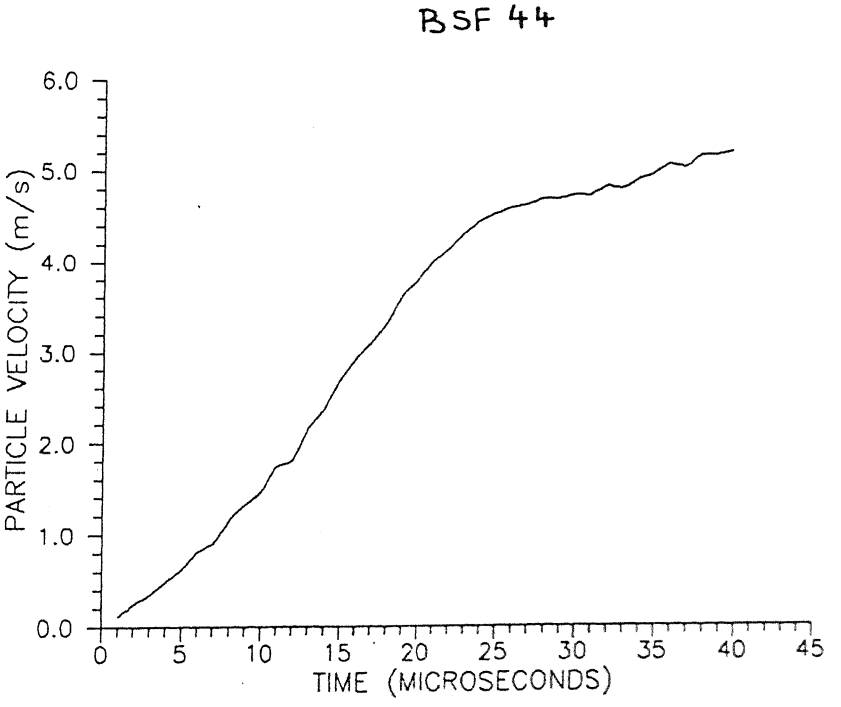

Fig. 5.24 (P-t) and (V-t) Relationship for Experiment BSF44

BSF47

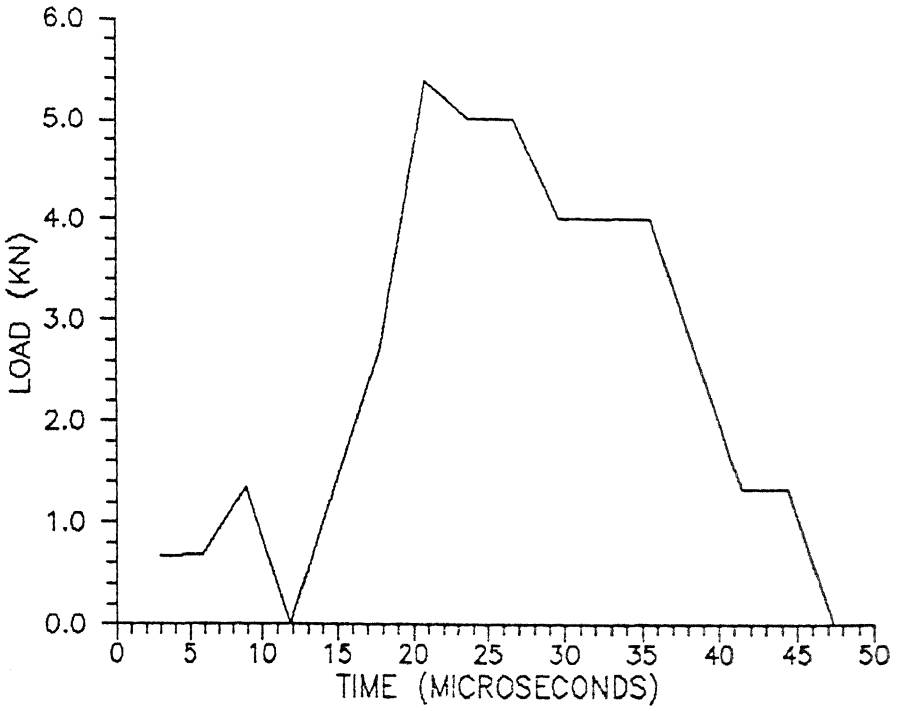
6.0
5.0
4.0
3.0
2.0
1.0
0.0
LOAD (KN)
0
5
10
15
20
25
30
35
40
45
50
TIME (MICROSECONDS)

BSF47

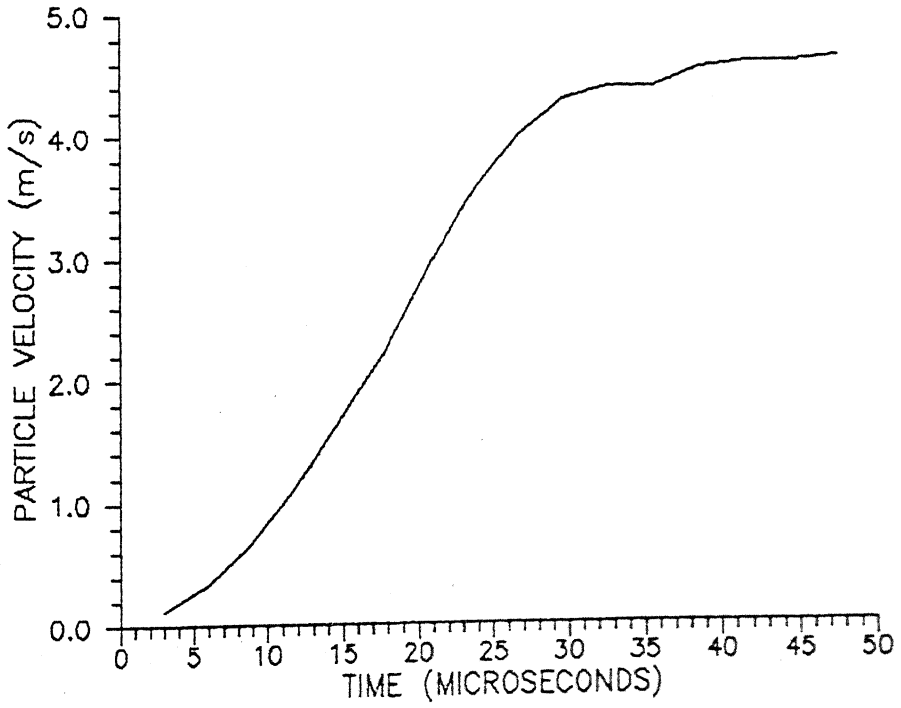
5.0
4.0
3.0
2.0
1.0
0.0
PARTICLE VELOCITY (m/s)
0
5
10
15
20
25
30
35
40
45
50
TIME (MICROSECONDS)

calculated by considering the total time taken between the first and last gauge drop recorded and the total distance travelled by the crack in between the drops. Using the relation (equation 5.12) the values of dynamic G^{D}_{IIC} are evaluated. The results of twelve experiments are tabulated in Table II. The average values of dynamic G^{D}_{IIC} obtained for the laminates A, B and C are 1022, 1598± 205, and 1693± 393 J/m^2 respectively.

5.6 G_{IIC} for a quasi-static case :

Carbon/epoxy specimens were tested in 3-point bending for a quasi-static case.The initial crack length was adjusted to 10mm and the span was kept at 50mm. The specimen loading was carried out in displacement control as shown in figure 5.26. The load range was upto 3 tons and load was increased at the rate of 10 Kgs/sec. A load versus displacement plot shows a linear increase until a sudden drop in the load occurs. This indicates that the crack has propagated. The slope of the load-displacement plot is determined.Its inverse gives the compliance C of the specimen. The G_{IIC} values are determined by [18]

$$G_{IIC} = \frac{9\,P^2 C\,a^2}{2b\,(2L^3 + 3a^3)}$$

where P is the applied load, C is the compliance of the specimen 2L is the span length, a is the crack length and b is the specimen width.

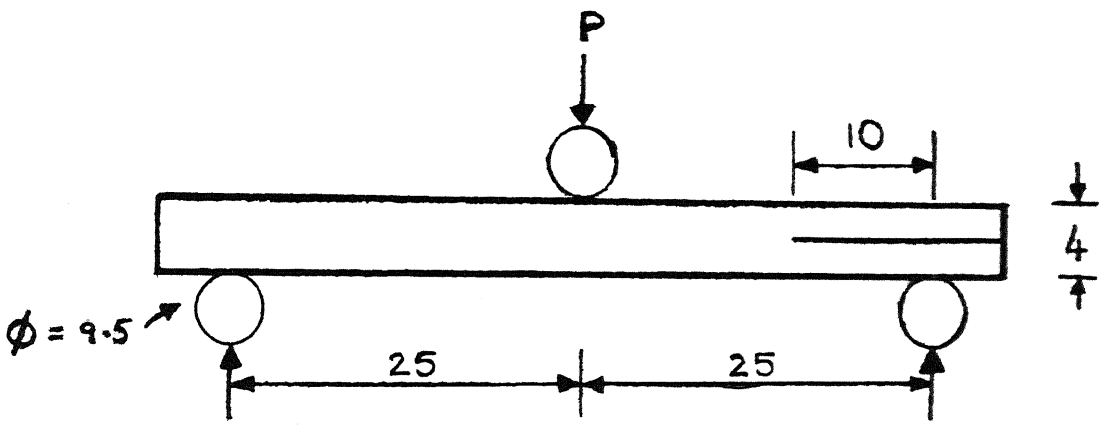

Fig. 5.26 3 - Point Bending of the Specimen
in a Quasi - static case

Table III gives a set of values for G_{IIC} in quasi-static conditions. The average value is 977 J/m^2.

5.7 Discussions :

On comparison of G_{IIC} in dynamic and quasi static conditions, the values for a dynamic case are higher (by a factor of 1.7) than those of quasi-static ones.

In literature so far, varied results have been presented. Sun et.al.[11] also found increased value of the dynamic values of G_{IIC} (by a factor of 5) as compared to the values in quasi-static case. Smiley[10] and Maikuma[12] reported a decrease in the values of G_{IIC} as the loading rate is increased.

In the work of other investigators, static or dynamic, a precrack was introduced between two like plies at the mid-plane of symmetric laminates. This was done to avoid coupling between bending and stretching at the expense of propagating cracks between two like plies. Infact, experimental evidences have shown that only rarely two plies of same orientation separate.Thus the results of other investigators may not be applicable to real life failures.

The present orientation code selected for experimentation satisfies both the conditions, i.e. its [B] matrix is null and an interface is possible with two symmetrical halves. This enables an investigator to study the behaviour of crack propagation at an interface.

TABLE - II

Expt No.	Shot No.	Crack Velocity (m/s)	Peak Load (KN)	Velocity Under Load (m/s)	$\frac{PV}{2ba}$ (J/m^2)	$\frac{dK}{da}$ (J/m^2)	G_{DC} (J/m^2)
1	BSF6	192	11.9	4.7	7187	6165	1022
2	BSF24	112	8.5	1.8	3483	2025	1457
3	BSF25	85	11.8	4.5	16541	14816	1725
4	BSF26	333	11.1	4.4	5726	4378	1348
5	BSF28	124	11.7	3.5	8080	6219	1851
6	BSF33	86	12.5	3.5	11527	9452	2075
7	BSF38	70	9.8	3.8	13520	11537	1983
8	BSF39	200	8.5	3.4	3639	2213	1426
9	BSF40	68	6.2	2.6	5785	4338	1447
10	BSF41	157	7.1	2.4	2733	1006	1727
11	BSF44	260	8.0	4.6	3556	1366	2190
12	BSF47	230	5.3	3.6	2039	1032	1007

Average value of dynamic G^D_{IIC} for laminate A = 1022 J/m^2

Average value of dynamic G^D_{IIC} for laminate B = 1598 ± 205 J/m^2

Average value of dynamic G^D_{IIC} for laminate C = 1693 ± 393 J/m^2

TABLE - III

Experiment Number	G_{IIC} (J/m^2)
1	1189
2	992
3	800
4	1093
5	900
6	1013

CHAPTER 6

CONCLUSIONS AND SCOPE FOR FUTURE WORK

The interlaminar fracture toughness values for G-808Carbon/Epoxy composites were determined experimentally under impact loading. Precracked ENF specimens were loaded in 3-point bending resulting in the crack extension in mode II. Unlike the work of other investigators,the configuration of the laminate enables an investigator to experimentally obtain the values of critical G_{IIC}since the crack propagates on an interface. The [B] matrix for the laminate is null. This is particularly important since most real life failures occur by delamination of laminates. The average value of G^{D}_{IIC}under dynamic conditions (1693 J/m^2) is higher by a factor of 1.7 as compared to corresponding values of G_{IIC} in quasi-static conditions.

In the present study, the values of energy release rate largely depend the accurate measurement of crack velocity. A more sensitive instrument (having a time scale of < 0.5μs) will give a better result.The material of the gauges also plays an important role in measuring the crack velocity.A carbon fibre is a good replacement for the copper wire since carbon is brittle. It has a low ultimate strain of 1.5% .Bonding of the gauges at an angle (as discussed in chapter 5) minimises the effect of cosine law.

REFERENCES

B.D. Agarwal and L.J. Broutman, "Analysis and Performance of Fibre Composites", Second Edition, John Wiley and Sons, New York, 1990.

G.R. Irwin, "Analysis of Stresses and Strains near the End of a Crack Traversing a Plate", Trans. ASME Journal of Applied Mechanics, Vol 24, 1957, pp 361-364.

A.A. Griffith, "The Performance of Rupture and Flow in Solids", Phil. Trans. Royal Soc. of London, A221, 1920, pp. 163-197

L.B. Freund, "Dynamic Fracture Mechanics", Cambridge University Press, Cambridge, 1990.

Ivana K. Partridge, "Advanced Composites", Elselvier Applied Science, London, 1989.

L.A. Carlsson, J.W. Gillespie(Jr.) and R.B.Pipes, "On the Design and Analysis of End Notched Flexure (ENF) Specimen for Mode II Testing", Journal of Composite Materials, Vol. 20, 1986, pp. 594-604.

G. Marom, I. Roman, H. Harel, M.Rosensaft, S. Kenig and M. Moshonov, "The Characterisation of Mode I and Mode II Delamination Failures in Fabric Reinforced Laminates", Proc. ICCM VI and ECCM 2, ed. F.L. Mathews, N.C.R. Buskell, J.M. Hodgkinson and J. Morton, Elsvier Applied Sciences, London 1987, pp. 3.265 - 3.273.

H. Maikuma, J.W.Gillespie (Jr.) and J.M.Whitney ,"Analysis and Experimental Characterisation of the Centre Notched Flexure Test Specimen for Mode II Interlaminar Fracture", Journal of Composite Materials, Vol. 23, (1989) pp. 756 - 786.

P. Davies, C. Moulin and H.H. Kausch, "Measurement of G_{IC} and G_{IIC} in Carbon/Epoxy Composites", Comp. Sc. and Tech., Vol. 39, 1990, pp. 193-205.

A.J. Smiley and R.B. Pipes, "Rate Sensitivity of Mode II Interlaminar Fracture Toughness in Graphite/Epoxy and Graphite/PEEK Composite Materials", Comp. Sc. and Tech., Vol. 29, 1987, pp. 1 - 15.

11. C.T. Sun and J.E. Grady, "Dynamic Delamination Fracture Toughness of a Graphite/Epoxy Laminate Under Impact", Comp. Sc. and Tech., Vol. 31, 1988, pp 55 - 72.

12. H. Maikuma, J.W. Gillespie (Jr.) and D.J. Wilkins, "Mode II Interlaminature Fracture of the Centre Notch Flexural Specimen under Impact Loading", Journal of Composite Materials, Vol. 24, 1990, pp 124-149.

13. A.R. Gawahale, "Fracture Toughness Behaviour of FRP's Reinforced by Aluminium Particles at the Interface", M.Tech. Thesis , I.I.T. Kanpur, 1990.

14. H. Kolsky, "Stress Waves in Solids", Dover Publications Inc., New York, 1963.

15. J.D. Achenbach, "Wave Propagation in Elastic Solids", North-Holland Pub. Co. , Amsterdam, 1973, P 241.

16. J.S.R.K.T. Prasad, "Experimental Evaluation of Dynamic Interlaminar G_{IC} of Glass Fabric Reinforced Epoxy Laminates", M.Tech. Thesis , I.I.T. Kanpur, 1990.

17. M.D. Narayan, "Energy Release Rates in Delamination of Glass Fabric Reinforced Composite Laminates", M.Tech. Thesis,I.I.T. Kanpur, 1988.

ME-1991-M-BAB-EXP.